AN ABSTRACT OF THE THESIS OF

Nimal K.K. Gamage for the degree of Master of Science in Atmospheric Science presented on March 7, 1986.

Title: Structure of Turbulence in Stratified Flow: Analysis of Data from SESAME and ALPEX.

Redacted for Privacy

Abstract approved: _____
Larry Mahrt

Several horizontal flight segments from SESAME and ALPEX are studied using structure functions and specral analysis methods. Theoretical analysis of the relative errors in structure function and correlation function in the presence of large scale wave activity is presented. The effect of stratification and shear on the -5/3 inertial subrange is noted. The expected ratio of horizontal velocity components for spectra and structure functions (4/3) is observed in the inertial subrange. The observed changes in the aspect ratio (defined as the square root of ratio of vertical velocity structure function to the mean horizontal velocity structure function) with turbulence strength and stratification are analysed.

Structure of Turbulence in Stratified Flow: Aircraft Data From SESAME And ALPEX

by

Nimal K. K. Gamage

A THESIS

submitted to

Oregon State University

in partial fulfillment of
the requirements for the
degree of

Master of Science

Completed March 7, 1986

Commencement June 1986

APPROVED:

Redacted for Privacy

Professor of Atmospheric Science in charge of major

Redacted for Privacy

Head of department of Atmospheric Science

Redacted for Privacy

Dean of Graduate School

Date thesis is presented March 7, 1986

Typed by researcher for Nimal K.K. Gamage

TABLE OF CONTENTS

LIST OF FIGURES

STRUCTURE OF TURBULENCE IN STRATIFIED FLOW: ANALYSIS OF AIRCRAFT DATA FROM SESAME AND ALPEX

1.0 INTRODUCTION

The analysis of stratified turbulence could be performed on three types of data, i.e. data gathered from laboratory experiments, (such as grid generated turbulence) data gathered from tower experiments (such as those reported by Nai-ping et. al.,1983) and data gathered from aircraft (see Mahrt ,1985). This study uses aircraft data gathered during the Severe Environmental Storms and Mesoscale Experiment (SESAME) conducted in Oklahama, USA, in April and May of 1979 and The Alpine Experiment (ALPEX) conducted in Europe in March of 1982.

In the first case intermittent turbulence is sampled at the top of a shallow nocturnal surface inversion layer. The underlying inversion layer contains little significant turbulence (Mahrt,1985). In the second case, turbulence is observed in a bora flow over the coastal range in northern Yugoslavia. Here, a wide variety of turbulent strengths can be studied at different levels.

Turbulence in geophysical flows generally occurs with a wide variety of other flows, such as internal gravity waves, two-dimensional turbulence and meandering. If the different flow phenomena are associated with distinctly different characteristics, such as scales, then it would be a relatively easy task to separate one flow from the other and study its characteristics in seclusion.

Turbulence measured in real flows is usually characterized by insufficient scale separation (significant turbulence and gravity waves may coexist at scales of a few hundred meters) and also yield similar characteristics for some statistics. For example, Weinstock (1978) considers the case of gravity waves and turbulence having similar spectral slopes. Hence, the analysis of such data requires careful consideration as to the kind of statistics to be computed and also the suitable values of cut-off frequencies etc. to be used in the evaluation of such statistics.

Previous studies have established certain physical processes that are occurring in geophysical flows. The shear induced overturning and subsequent break down to smaller scales, acts as the main source of energy to the shear induced turbulence (Tennekes and Lumley ,1972). This energy is transferred by different processes to the dissipating scales to be converted to heat through viscous dissipation.

Kolmogorov (1941) hypothesized that this energy transfer occurs through an inertial regime where the energy was conveyed through a "pipeline" from the small wave number source region to the large wave number sink region. He also found through the use of dimensional analysis that the energy spectra in this region should obey a -5/3 power law dependence on wave number. Since the energy transfer and the dissipation should be equal for equilibrium, he used the wave number and dissipation rate as the variables in this dimensional argument. Subsequent researches have looked at cascades of enstrophy (Lilly 1983, Gage and Nastrom 1985) and ensuing spectra.

The overall picture looks as follows. The input energy is dissipated in the viscous subrange, also called the dissipation range, while a fraction of it may be transmitted to large scale, possibly two-dimensional, vortices. This upscale transfer of energy may lead to slopes steeper than -5/3 predicted by Kolmogorov (see Gage and Nastrom 1985, Weinstock 1980). Two dimensional vorticity would display a -3 slope (Lilly 1983) or a -5/3 slope (Kraichnan 1967). In between the inertial region and the wave region may lie the buoyancy subrange (Weinstock

1978), sometimes manifesting itself as a hump in the spectra. Vinnichenko (1970) suggested three possible spectral slopes for the bridge between mesoscale activity and microscale activity as considered by Kolmogorov. Weinstock (1980) suggested that the steepening of spectra between the meso and micro scales is a catch-up region.

In addition to the above transfer processes is the actual position and size of the energy containing eddies in the flow realization. In shear generated turbulence the possibility of Kelvin-Helmoltz waves exist. Such rolls or eddies lie with their vortex lines across the direction of shear, and are characterized by circulation in the direction of shear (Fig 1.1). Townsend (1970, 1976) suggests the existence of double roller eddies, which are counter rotating, lying in the direction of shear (Fig.1.2)

In a later study, Moin and Kim (1984) suggest that these eddies be inclined to the shear and further suggest the existence of hair pin like structures caused by the twisting of cross stream vortex lines by the shear. Fig.(1.3) shows the direction of the vorticity vectors in a plane inclined to the shear. The shading indicates the hairpin like structures.

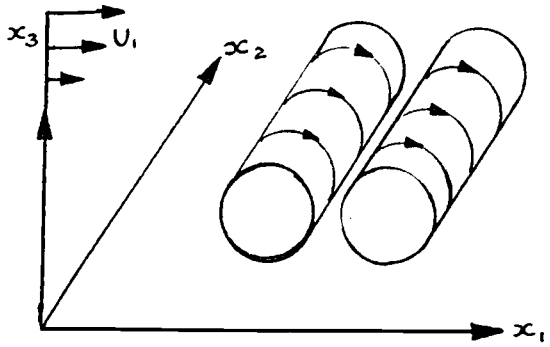

Fig. (1.1) Rolls Accross The Shear

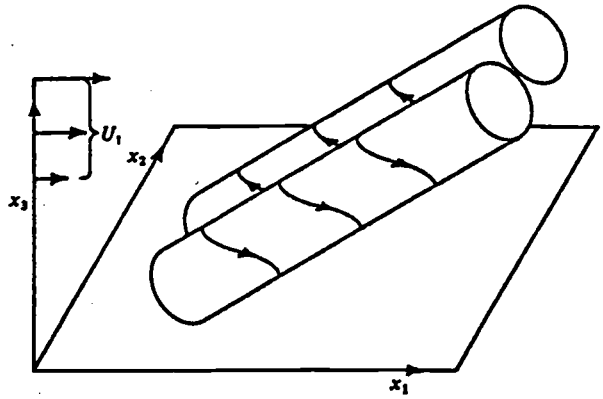

Fig. (1.2) Rolls Aligned with the shear

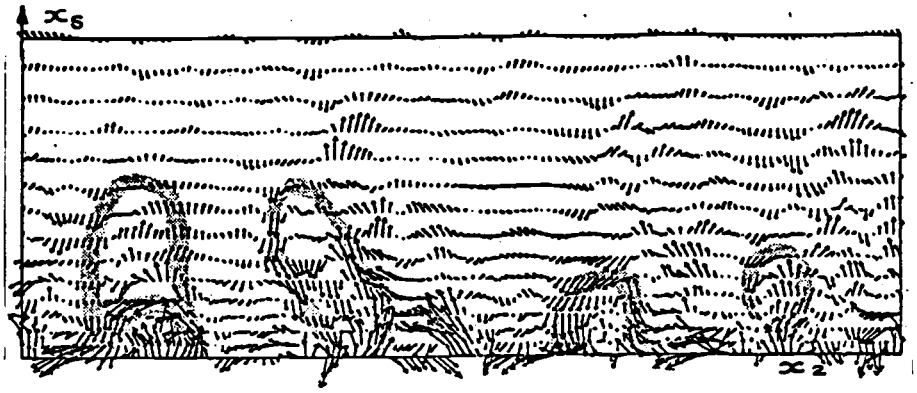

Fig. (1.3) Hairpin Vortices Causing Rolls
From Moin and Kim (1985)
Arrows indicate vorticity vectors on shear plane

This study tries to use different statistical tools to visualize the physical processes causing the turbulence and also compares the result with previous work. In chapter two the theoretical tools used are described. This is done in two parts. Part 1 describes the traditional methods such as spectra and correlation methods. Part 2 describes the structure function methods used extensively in this work. The final part of this chapter deals with comparisons of structure function methods with spectral methods with various advantages and disadvantages detailed.

Chapter three presents the results obtained by analyzing the data. Here the data analysis with spectral methods are compared with the structure function results. Chapter four describes the possible physical processes as envisioned from the analysis. It also compares these results with previous work.

2.0 DESCRIPTION OF METHODS OF STATISTICAL REPRESENTATION

This chapter deals with the mathematical analysis of the various statistical tools that will be used in the analysis of data.

2.1 Description of the theoretical development of spectra and co-spectra.

An observed velocity (or any other variable) component u(x) will be made up of the mean U(x) and the turbulent component u'(x), such that ,

$$u(x) = U(x) + u'(x) \qquad (2.1.1)$$

Further, let the process u(x) be stationary with U(x) being removed from the record (by means of a low-pass filter). Then, the correlation function of the process is defined by,

$$B(r) = E[\, u(x).u(x+r) \,]$$
$$= \langle\, u(x).u(x+r) \,\rangle \qquad (2.1.2)$$

Where E is the expected value, and

$\langle\ \rangle$ denotes the average over the whole record.

In the case of a stationary random process (as in the case u(x)) the correlation function depends only on lag r. Also from Schwartz's inequality, for the above process,

$$B(r) \leq \text{sqrt.}(E[u(x)^2].E[u(x+r)^2]) \leq (\text{std. dev. } u)^2 \qquad (2.1.3)$$

B(0) is twice the specific kinetic energy of the process.

Now the Fourier transform of the correlation function, B(r) yields,

$$F(k) = (1/8\pi^3) \int \exp(-ikr)\ B(r)dr \qquad (2.1.4)$$

F(k) is defined as the spectral energy density of the process. Taking the inverse transform of (2.1.4)

$$B(r) = \int \exp(ikr)\ F(k)dk \qquad (2.1.5)$$

The spectrum $E(k) = \int_{|\underline{k}|=K} F(k)dk$ (2.1.6)

Combining (2.1.5) and (2.1.6), for r = 0

$$B(0) = \int E(k)dk \qquad (2.1.7)$$

In the case of homogeneous and isotropic fields the above equations can be written as

$$B(r) = 2\int (\ \sin(kr)/kr\ )\ E(k)dk \qquad (2.1.8)$$

For a one dimensional random variable

$$B(r) = \int \cos(kr)\ E(k)dk \qquad (2.1.9)$$

For the multidimensional case, equations (2.1.1) to (2.1.9) can be redefined as follows:

The cross correlation function for the two variables u(x), v(x) is defined as

$$B_{uv}(r) = \langle u(x+r).v(x) \rangle$$

Since the process is still a stationary process the cross correlation function is dependent only on the spatial separation, r. The Fourier transform of the cross correlation function is called the cross-spectrum and denoted by $F_{uv}(k)$.

2.2 Description of the theoretical development of statistics of increments.

We shall begin with a process(es) of the single variable x (a similar development can be done for the case where x is replaced with X, the three dimensional spatial vector, or t, time in the case of a time series.).

2.2.1 The first property of interest is the First Moment m(x,r), defined as,

$$m(x,r) = \langle u(x+r) - u(x) \rangle \qquad (2.2.1)$$

calculated over different values of r.

where, u(x) is the variable of interest,

and r is the spatial separation over which gradients are computed.

< > denotes average over all samples in the record.

Also of interest is the distribution of finite gradients J(r), defined as the differences computed over the separation distance r. Inspection of J(r) would provide information on the dominant gradient for a given scale (scale meaning the separation r in time or space).

m(x,r) would provide information on regions of strong gradients over the scale r.

2.2.2 The second property of interest is the Structure Function of the random variable u(x) defined as, (see Doviak and Zrnic, 1984 or Monin and Yaglom, 1975)

$$D(r) = \langle (u(x+r) - u(x))^2 \rangle \qquad (2.2.2)$$

Where, < > denotes average over all samples in a record. By definition the structure function is non-negative and even.

Further, $D(0) = 0.0$

Now , if the process is stationary, and if $\langle u(x) \rangle = 0.0$,

$$D(r) = \langle (u(x+r) - u(x))^2 \rangle$$
$$= 2 \langle u(x+r)u(x+r) \rangle - 2 \langle u(x+r)u(x) \rangle$$
$$= 2 (B(0) - B(r)) \qquad (2.2.3)$$

Where B(r) is the co-variance function defined in section 2.1 as ,

$$B(r) = \langle u(x+r)u(x) \rangle .$$

Equation (2.2.3) can be also written as

$$D(r) = 2 B(0) (1 - B(r)/B(0)) \qquad (2.2.4)$$

2.2.3 Since $-1 \leq B(r)/B(0) \leq +1$ (as shown in 2.1)

Eqn.(2.2.4) gives $0 \leq D(r) \leq 4 B(0)$ (2.2.5)

Hence, the structure function has an upper and a lower bound.

Since B(r) becomes zero at large separation distances, due to the fact that points far apart are not influencing one another,

$$D(r) \longrightarrow 2 B(0) \text{ at large } r. \qquad (2.2.6)$$

Fig(2.1) shows some typical correlation functions and their corresponding structure functions.

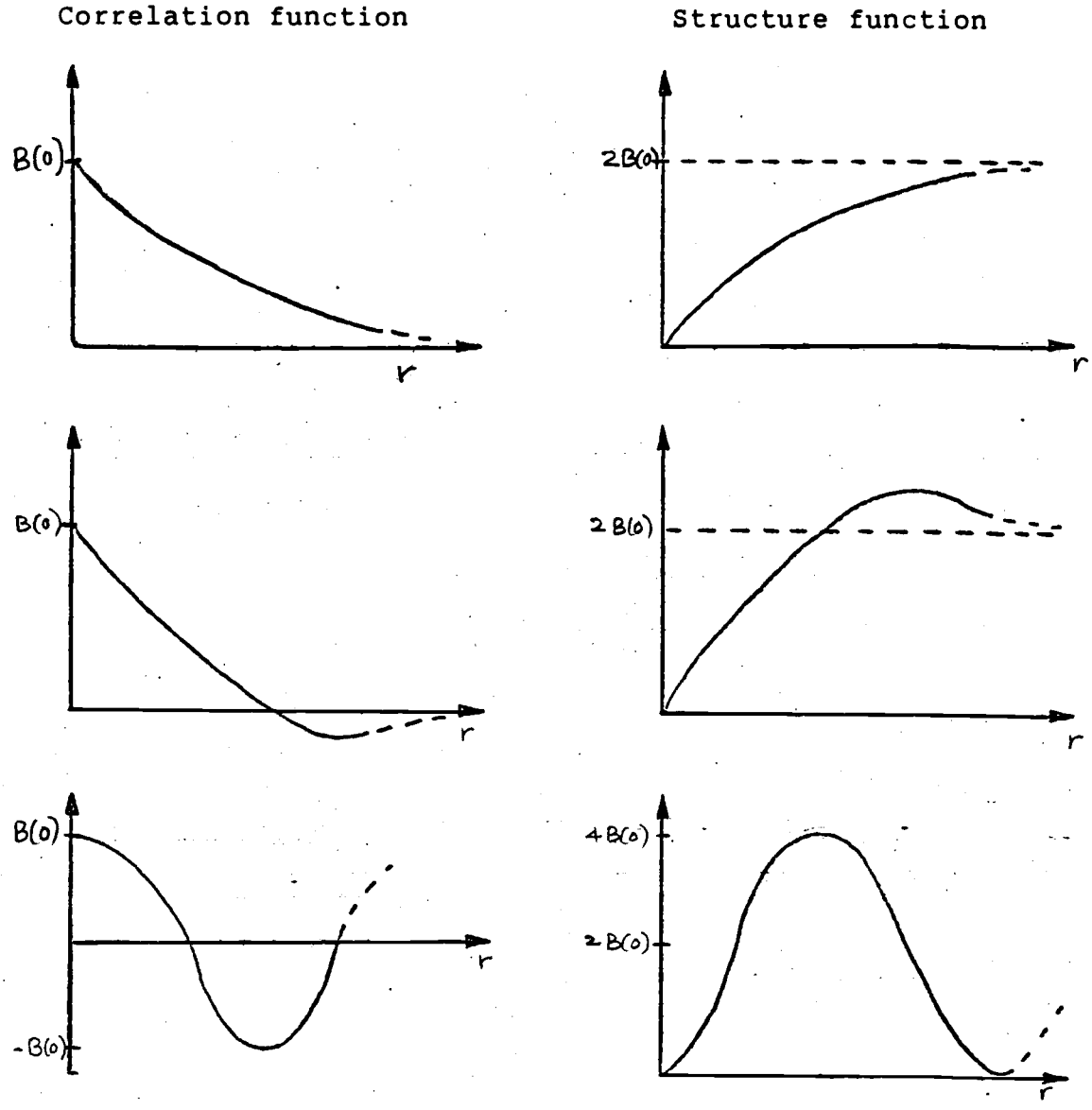

Fig.(2.1) Typical correlation functions with corresponding structure function

Let us consider the expression in equation (2.2.2).

$$D(r) = \langle (u(x+r) - u(x))^2 \rangle$$

$$= \langle (\sum_{i=1}^{n} (u(x+ir/n) - u(x+(i-1)r/n)))^2 \rangle$$

Here i is the smallest sub-interval within r. In practice this would be the resolution (minimum space between samples) of the measuring instrument (fig. (2.2)). n is the number of sub-intervals within r.

Using Schwartz inequality and following the approach of Monin and Yaglom (1975), the above can be rewritten as

$$D(r) \leq \sum_{i=1}^{n} \sum_{j=1}^{n} \langle (u(x+ir/n) - u(x+(i-1)r/n)^2) * (u(x+jr/n) - u(x+(j-1)r/n)^2) \rangle$$

$$\leq n^2 (D(r/n) \qquad (2.2.7)$$

Where D(r/n) is the structure function for the resolution of the measuring instrument, r/n.

The above equation can be rewritten as

$$D(r)/r^2 \leq D(r/n)/(r/n)^2$$

Or $$D(r)/r^2 \leq A \ , \qquad (2.2.8)$$

where A is the maximum of the bounded structure function D.

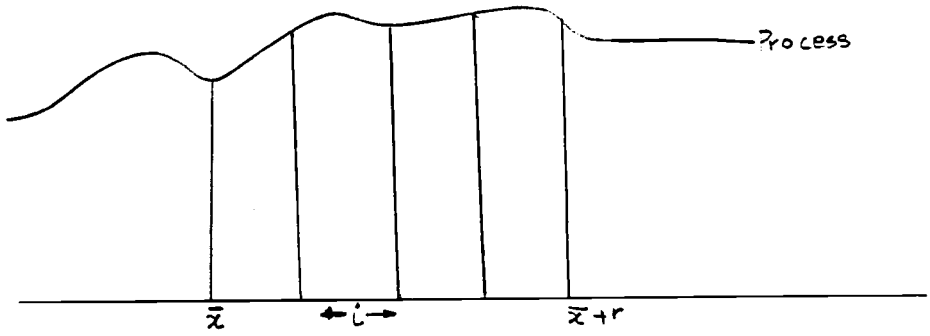

Fig.(2.2) Resolution of a record

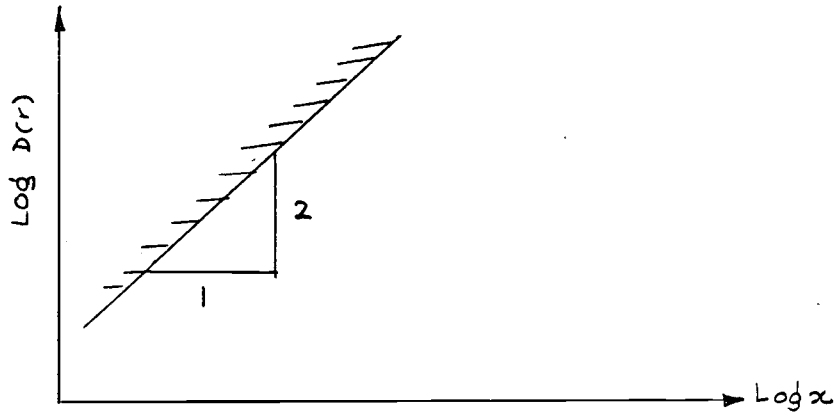

Fig.(2.3) Region of possible structure functions

Hence the structure function $D(r) \leq Ar^2$. (If the variable of interest is a linear function of x then the structure function takes this form.) Hence it is shown that the structure function cannot rise more rapidly than r^2. See fig.(2.2).

Also useful is the relationship between the structure function and the spectrum,

(i) For the case of three-dimensional isotropic flow , combining (2.1.8) and (2.2.3) ,

$$D(r) = 2 \int (1 - \sin (kr)/kr)\, E(k)dk \qquad (2.2.9)$$

(ii) For the case of one-dimensional homogeneous flow, combining (2.1.9) and (2.2.3) ,

$$D(r) = 2 \int (1 - \cos kr)\, E(k)\, dk \qquad (2.2.10)$$

where , $B(0) = \int E(K)\, dK$. The one dimensional spectrum being E(k).(as defined in section 2.1)

If the energy spectrum E(k) is assumed to obey a power law in wave number such as

$$E(k) \propto k^{-n},$$

substituting for E(k) in 2.2.10 above,
(as in Babiano, et. al., 1985)

$$D(r) = 4 \int \sin^2(kr/2)\, E(k)\, dk$$

$$\propto 4r^{n-1} \int \sin^2(u/2)\, u^{-n}\, du$$

$$\propto r^{n-1} \quad \text{when} \quad 1 \leq n \leq 3 \qquad (2.2.11)$$

$$\propto r^2 \quad \text{when} \quad 3 < n \qquad (2.2.12)$$

Eqn.2.2.12 is obtained directly from eqn.(2.2.8), where it was shown that the structure function cannot rise faster than r^2.

2.2.3 The Co-structure function of a multidimensional random process is defined as

$$D_{uv}(r) = \langle (u(x+r)-u(x))(v(x+r)-v(x)) \rangle \qquad (2.2.13)$$

Where u,v are the two variables of interest.

$$D_{uv}(0) = 0.0 \qquad (2.2.14)$$

Unlike the structure function the Co-structure function can take negative as well as positive values though it is still an even function. It can be shown that the Co-structure function is related to the co-spectrum as

$$D_{uv}(r) = 2 \int (1 - \cos kr)\, E_{uv}(k)\, dk$$

Where $E_{uv}(k)$ denotes the cross spectrum.

2.3 Statistical representation of some theoretical functions and their traces.

In order to study the effect of sharp edges on the computed statistics a series of artificial records are analyzed (fig 2.4). It is observed that for the case of a sine curve the spectrum gives a single peak while the structure function follows a $\sin^2$ curve of half the wave length. For a square pulse wave the spectra contained several peaks (one at the wave length and others at smaller scales) and appeared to spread the energy over a wave length band. The structure function for this case is a triangular wave. The addition of white noise affected both the structure function and spectra similarly, i.e by addition of equal amount of energy at all scales.

Thus it is seen that the structure function is smoother than the spectrum for records with sharp boundaries while the spectra behave better for records made of periodic sinusoidal curves.

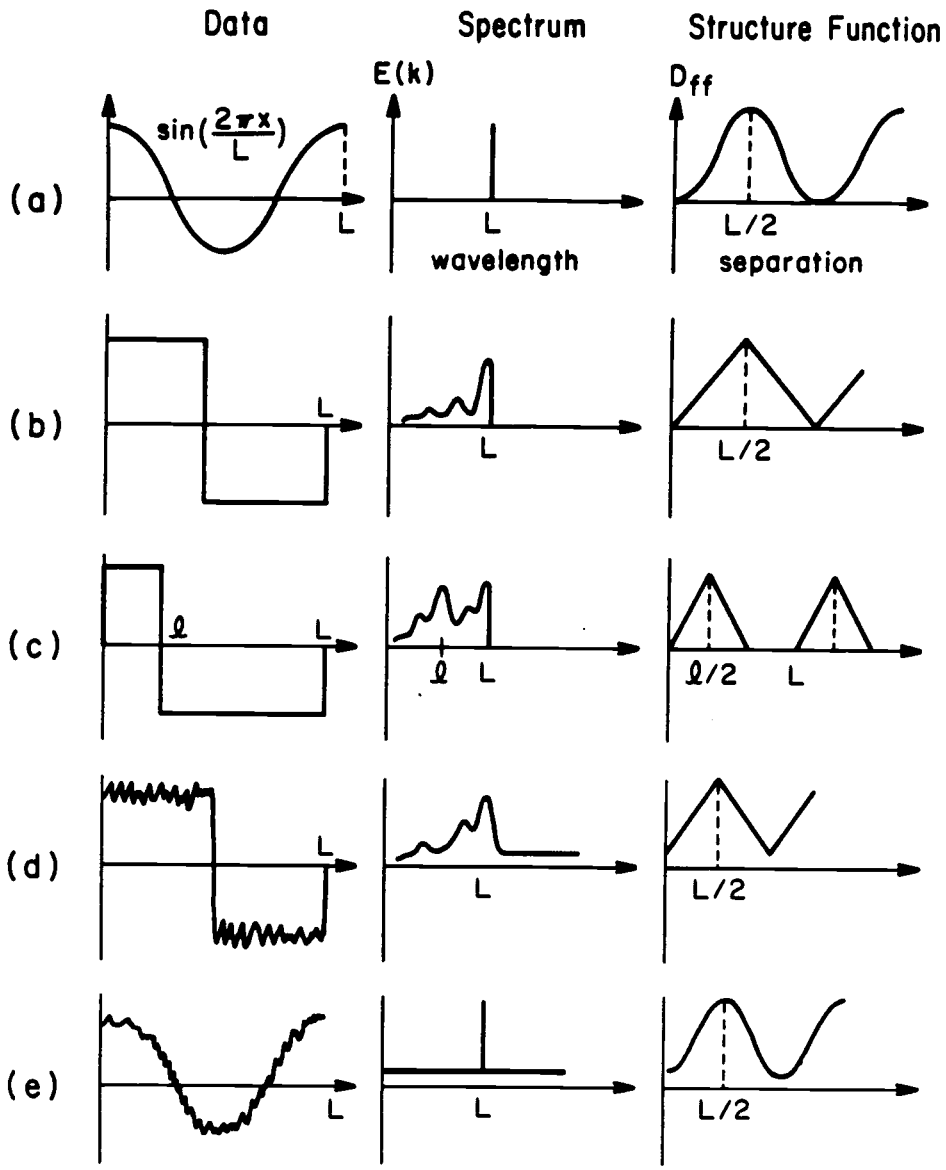

Fig. (2.4) Statistics of some artificial records

2.4 Comparison of effects of the nature of turbulence

Geophysical data containing turbulence has a very complex nature. The data is often intermittent and even in situations where the turbulence is caused by strong shear or convective heating, varies spatially. Imagine that the data would be partitioned into a slowly varying component such as gravity waves and a rapidly varying turbulent part. However in actuality the slowly varying components and the rapidly varying components are not well separated in scales and cannot be easily isolated from one another. Here the effects of two characteristics, namely, the effect of trend and the effect of the waves will be discussed. Presumably the real data records will have characteristics which are a mixture of the above two. (See Lumley and Panofsky, 1964).

2.4.1 Effect of trend on the computed statistics.

Here we consider a random process made up only of a statistically independent slowly varying component F(x) and a rapidly varying component f(x). We further assume the process to be stationary with zero mean (fig (2.5)). The record length is X and the lag used to compute the statistics is r.

From the definition of the correlation function in section 2.1, we obtain for this case,

$$B(r) = \langle (F(x+r)+f(x+r)).(F(x)+f(x)) \rangle \quad (2.4.1)$$

$$= \langle F(x+r).F(x) \rangle + \langle f(x+r).f(x) \rangle$$

$$= \quad (I) \quad + \quad (II) \quad (2.4.2)$$

The cross correlation terms in 2.4.1 are assumed zero. If the record is short enough, the slowly varying part could be assumed to be linear, as shown in fig(2.5). The product, $\langle f(x+r).f(x) \rangle$ is the correlation function due to the turbulence alone.

Substituting for (I) and (II) in (2.4.2)

$$B(r) = 1/X \int_{-X/2}^{X/2} F'.\ x.\ F'.(x+r)\ dx + B_f\ (r)$$

$$= F'^2.(X^2/12) + B_f(r)$$

= Error due to trend + Correlation due to turbulence

Where F′ is the derivative of F.

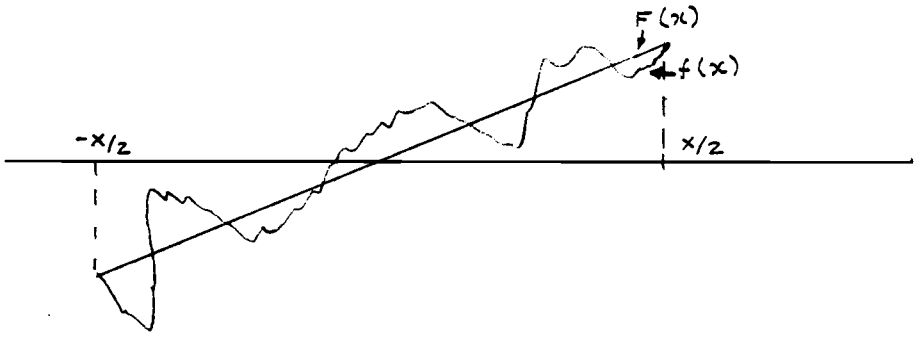

Fig.(2.5) Random process made of trend and turbulence

From the definition of the structure function in section 2.2 we obtain for this case,

$$D(r) = \langle (F(x+r)+f(x+r) - F(x) - f(x))^2 \rangle \qquad (2.4.3)$$

$$= \langle (F(x+r)-F(x)^2 \rangle + \langle (f(x+r)-f(x))^2 \rangle$$

$$= \quad (I) \qquad\qquad (II)$$

where (I) is the effect of the trend and (II) the structure function due to the turbulence. < > denotes an average over the record length. Following the analysis for the correlation function,(as in Lumley and Panofsky, 1964)

$$D(r) = F'^2\, r^2 + D_f(r)$$

$$= \text{Error due to trend} + \text{Structure function due to turbulence}$$

Using (2.2.3) the above can be re-written as

$$D(r) = 2\,B(0)\,[\,1 - B_f(r)/B(0)\,] + F'^2 .\, r^2$$

For all cases where the lag is smaller than a fourth of the record length the absolute error (trend contribution) in the structure function is smaller than that of the correlation function.

(The error in the structure function is smaller than $(F'^2X^2/16)$ while in the correlation function it is $(F'^2X^2/12)$.)

As r increases B(r) decreases. Hence the relative error due to trend increases in the correlation function. The value of the structure function increases with increasing r. Since B(0) > B(r), the relative error decreases in the structure function with increasing r.

Thus it is seen that the structure function is less influenced by the slowly varying components such as trend.

2.4.2 Effect of waves on computed statistics.

From equation (2.4.2) and (2.4.3) above, it is seen that the contribution due to the turbulence and due to the trend are given by II and I respectively. If we consider a case of a turbulence record in which wave activity is present (for the moment assumed as one wave number) and assume that the waves and turbulence have cross correlation coefficients of zero then, eqns.(2.4.2) and (2.4.3) are valid for this case.

Substituting $F(x) = a \sin(kx)$ in Eqn. (2.4.2)

See Fig.(2.4)

$$B(r) = 1/X \int a^2 \sin(kx) . \sin k(x+r) dx + B_f(r)$$

$$= a^2/X \int \sin^2(kx) dx \int (\sin(kx) . \sin k(x+r) dx / \int \sin^2 kx \, dx) + B_f(r)$$

$$= C \cos(kr) + B_f(r) \qquad (2.4.4)$$

Note:(i) $\sin(kx) . \sin k(x+r) dx / \sin^2 kx \, dx$ is the corelation function for a sin curve.

(ii) C is a constant equal to $(a^2/X) \sin^2(kx) \, dx$

Using Eqn.(2.4.3) and substituting for F(x),

$$D(r) = 1/X \int a^2 (\sin k(x+r) - \sin kx)^2 dx + D_f(r)$$

$$= 4C \sin^2(kr/2) + D_f(r) \qquad (2.4.5)$$

Using Eqn. (2.2.3) the above can be rewritten as

$$D(r) = 4C\sin^2(kr/2) + 2B_f(0)(1 - B_f(r)/B_f(0)) \qquad (2.4.6)$$

In order to compare the effect of the waves on the statistics a functional form has to be assumed for B_f.

If $B_f(r) = B_f(0) . e^{-kr}$

Then the relative error in the correlation equation (2.4.4) is given by

$$Error_{correlation} = C/B_f(0) . \cos(kr)/e^{-kr}$$

and for the structure function equation (2.4.6)

$$Error_{structure} = C/B_f(0) . \sin^2(kr/2) /(1-e^{-kr})$$

From Table 1 the relative error for the structure function is seen to be small compared with that of the correlation function.

The above analyses can easily be extended to the more general case of many wave lengths. Hence it is seen that in geophysical flow situations where both trend and wave activity is present the structure function at small scales is less influenced by them.

Table 1:Comparison of errors from correlation and structure functions for record made of waves and turbulence

kr	$\frac{\cos kr}{e^{-kr}}$	$\frac{\sin^2(kr)}{(1-e^{-kr})}$
0.1	1.0996	0.0525
0.2	1.1971	0.1100
0.3	1.2896	0.1723
0.4	1.3741	0.2394
0.5	1.4469	0.3111
0.6	1.5039	0.3871
0.7	1.5402	0.4671
0.8	1.5505	0.5508
0.9	1.5289	0.6376
1.0	1.4687	0.7272

3.0 ANALYSES OF DATA

Six cases are analyzed from each of the mornings of 5th and 6th May 1979 in SESAME and 22 cases from the bora flow of 6th March 1982 in ALPEX. These segments were made by selecting horizontal, turbulent sections of flights, which are typically about 12 km and 30 km long in SESAME and ALPEX respectively.

The data have been analyzed using two types of statistics, i.e spectral statistics, discussed in 3.1, and statistics of increments, discussed in 3.2. Upon computation of statistics, the results have been composited in groups of varying turbulence strengths. In the SESAME case the six segments of 5th May have been composited together and the segments of 6th May composited separately. Since the wind shear was much stronger on the 6th, composite S1 (SESAME 5th May) contains weaker turbulence than composite S2 (SESAME 6th May). The 22 segments from ALPEX have been composited into three groups: AS, AM and AW containing the strong, moderate andweak turbulence segments respectively.

3.1 Computation Of Spectral Statistics.

For the purpose of computation of statistics, the aircraft time was converted to distance using constant aircraft speeds of 80 m/s for SESAME and 120 m/s for ALPEX. This may result in slight over or under estimations on the order of 10%.

The data were linearly detrended before computation of any of the spectral statistics. The spectra, co-spectra and quadrature were computed using a Fast Fourier technique. For the purpose of constructing the composites each statistic was averaged at each wave number. The averaging process equally weighted the segments making up a composite.

The composite plots of power spectra are in fig (3.1.1 to 3.1.20).

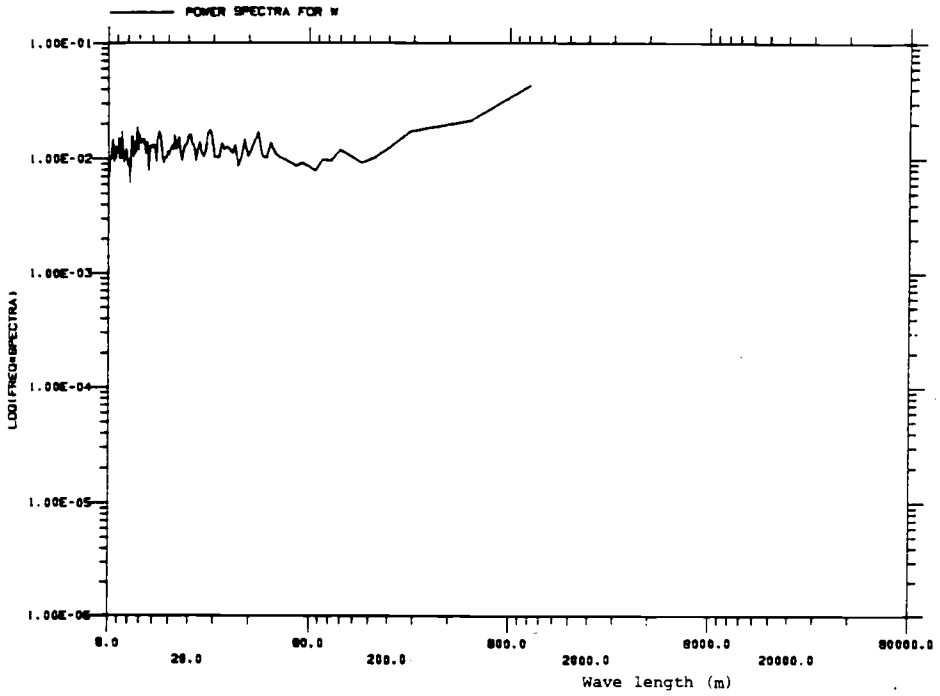

Fig. (3.1.1) Power Spectra of W

SESAME 5 th May

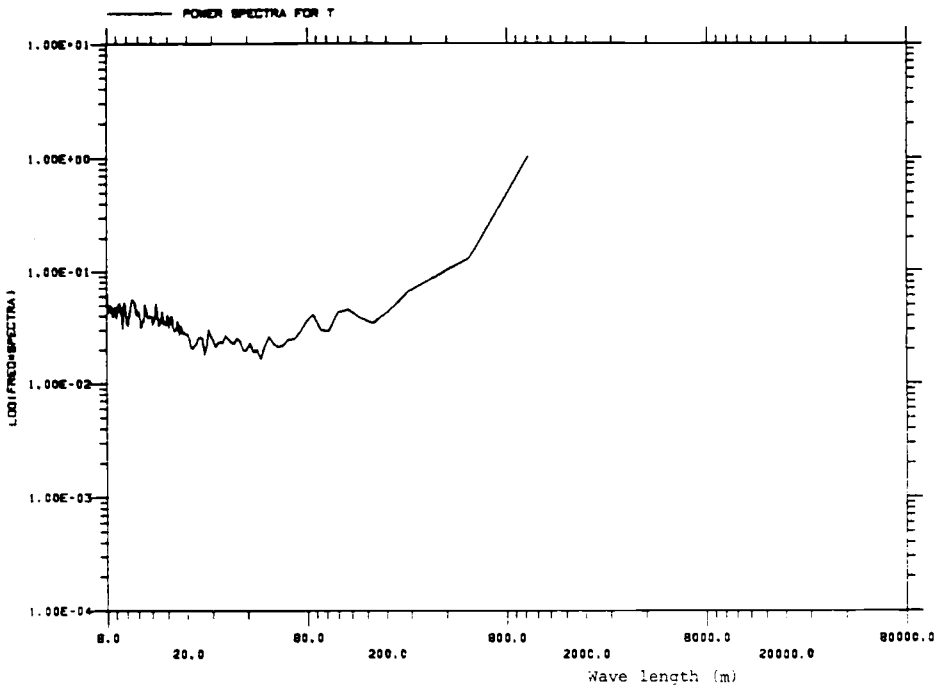

Fig. (3.1.2) Power Spectra of T

SESAME 5 th May

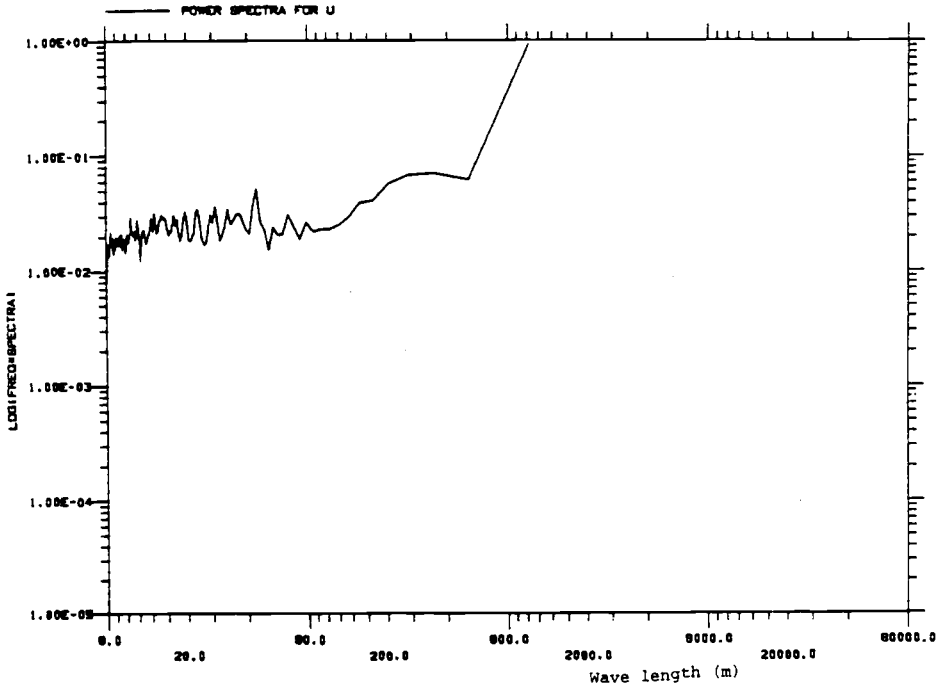

Fig. (3.1.3) Power Spectra of U

SESAME 5 th May

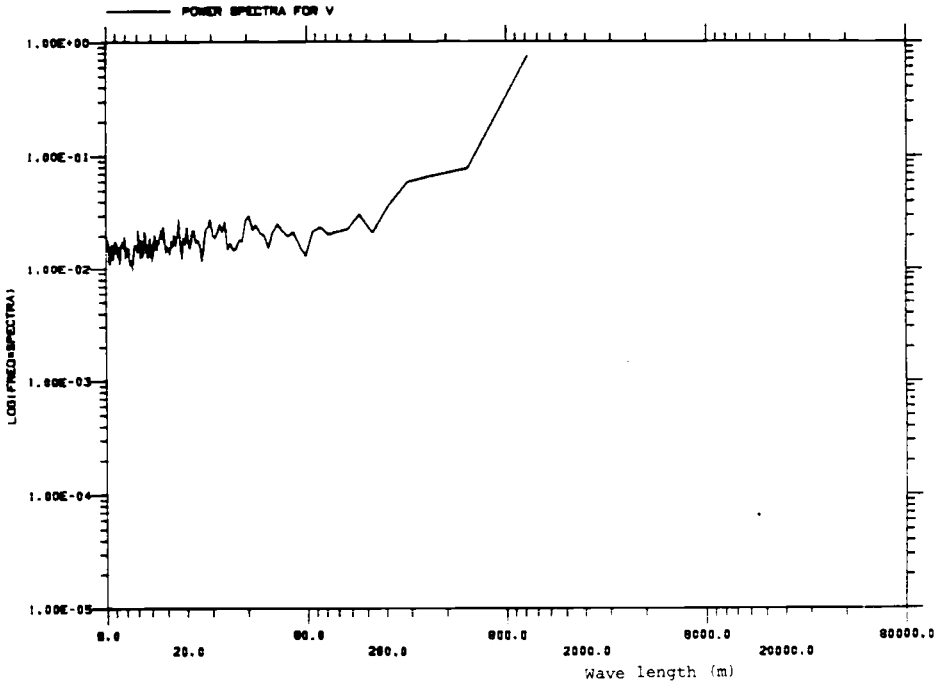

Fig. (3.1.4) Power Spectra of V

SESAME 5 th May

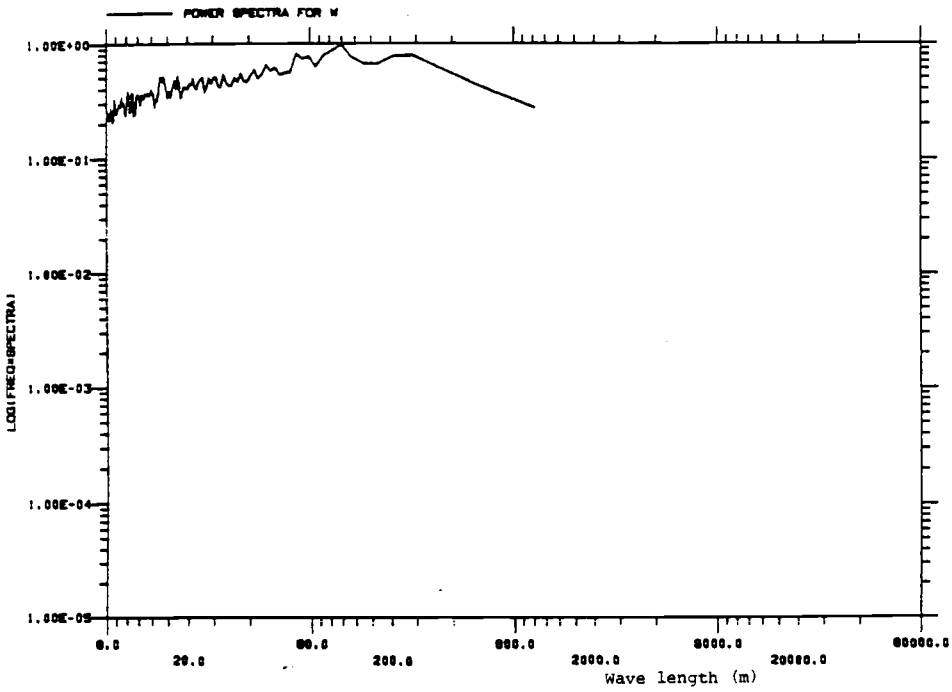

Fig. (3.1.5) Power Spectra of W

SESAME 6 th May

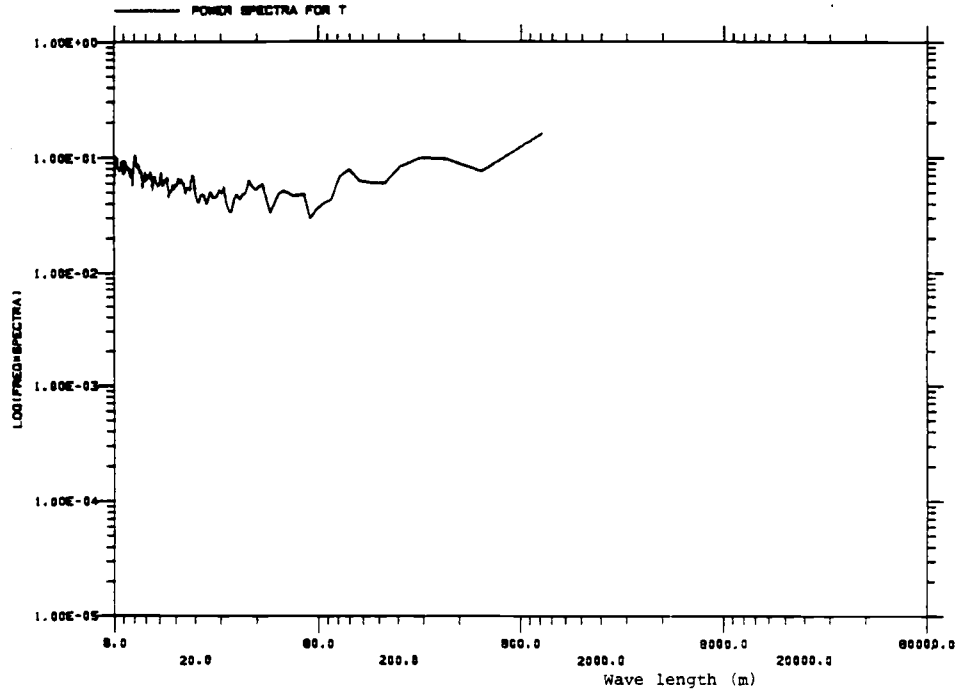

Fig. (3.1.6) Power Spectra of T

SESAME 6 th May

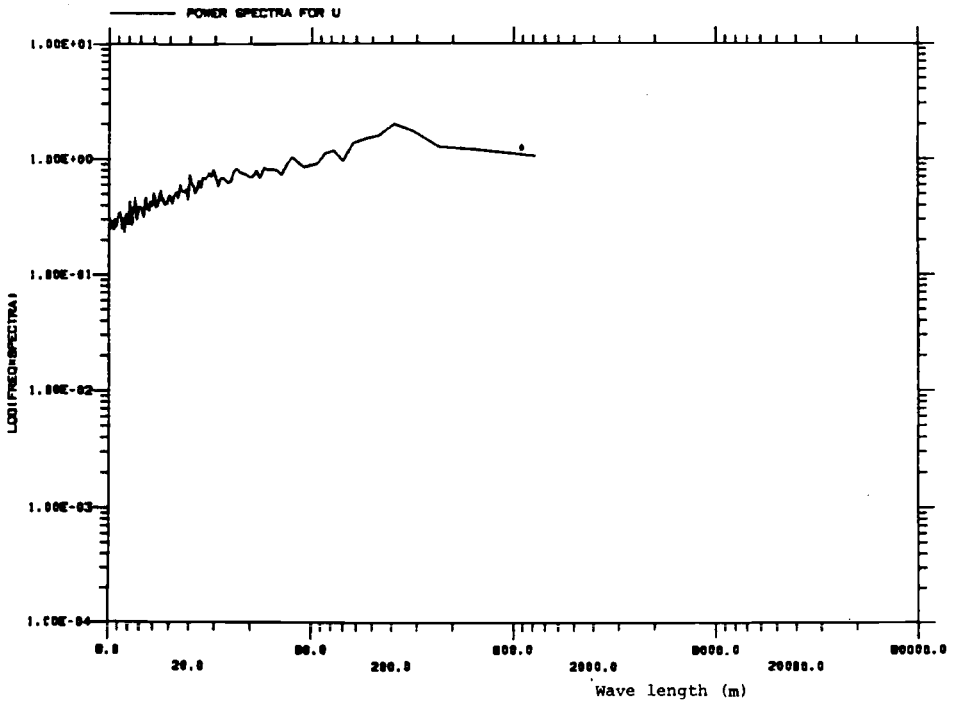

Fig. (3.1.7) Power Spectra of U

SESAME 6 th May

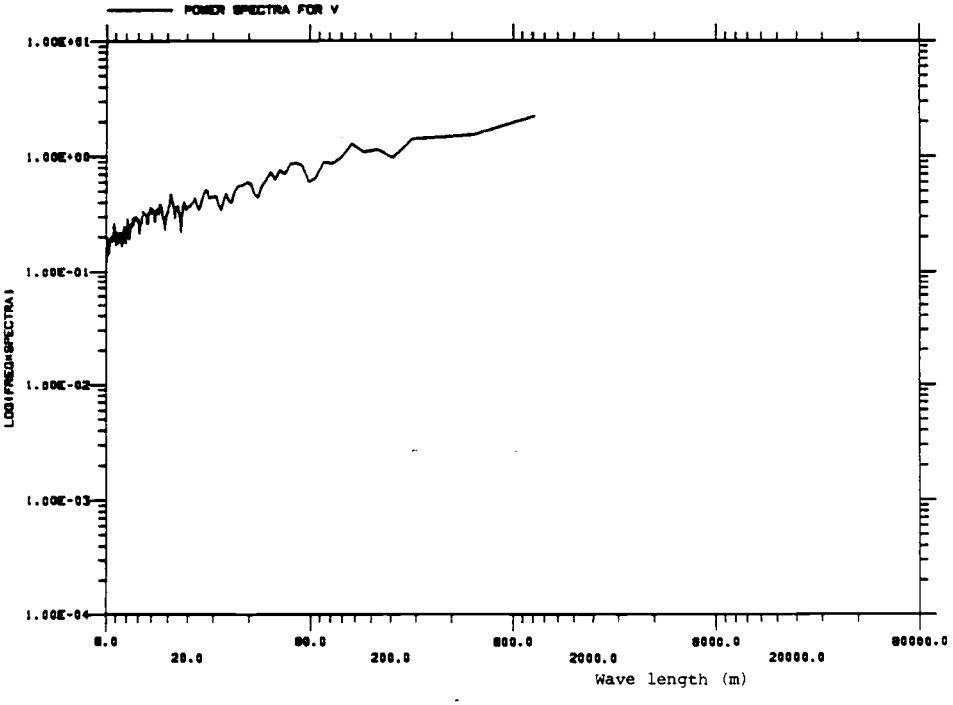

Fig. (3.1.8) Power Spectra of V

SESAME 6 th May

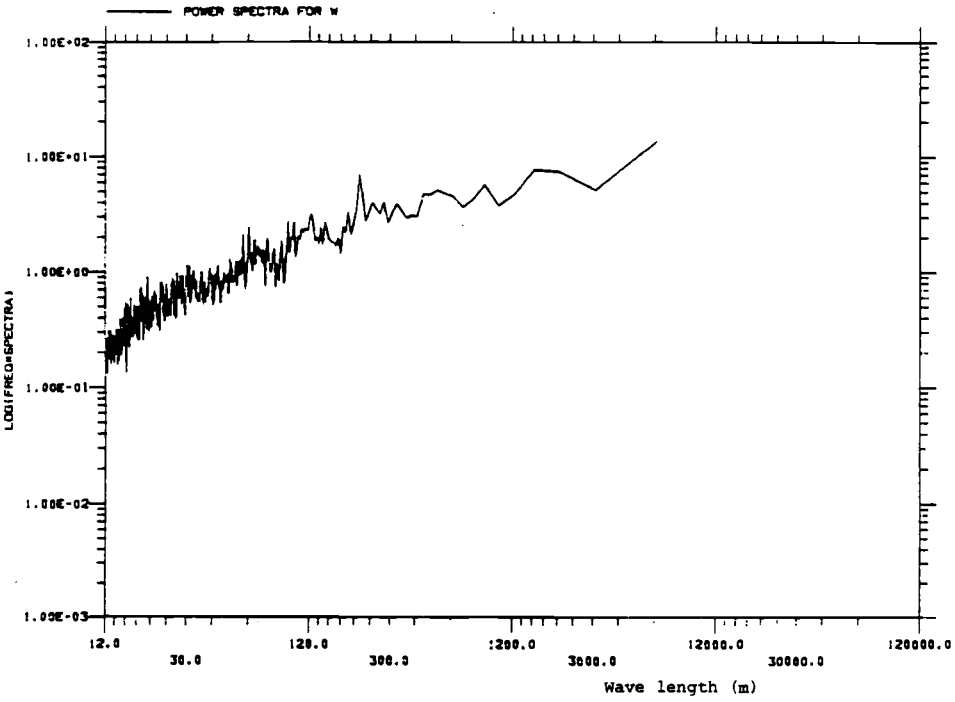

Fig. (3.1.9) Power Spectra of W

ALPEX STRONG COMPOSITE

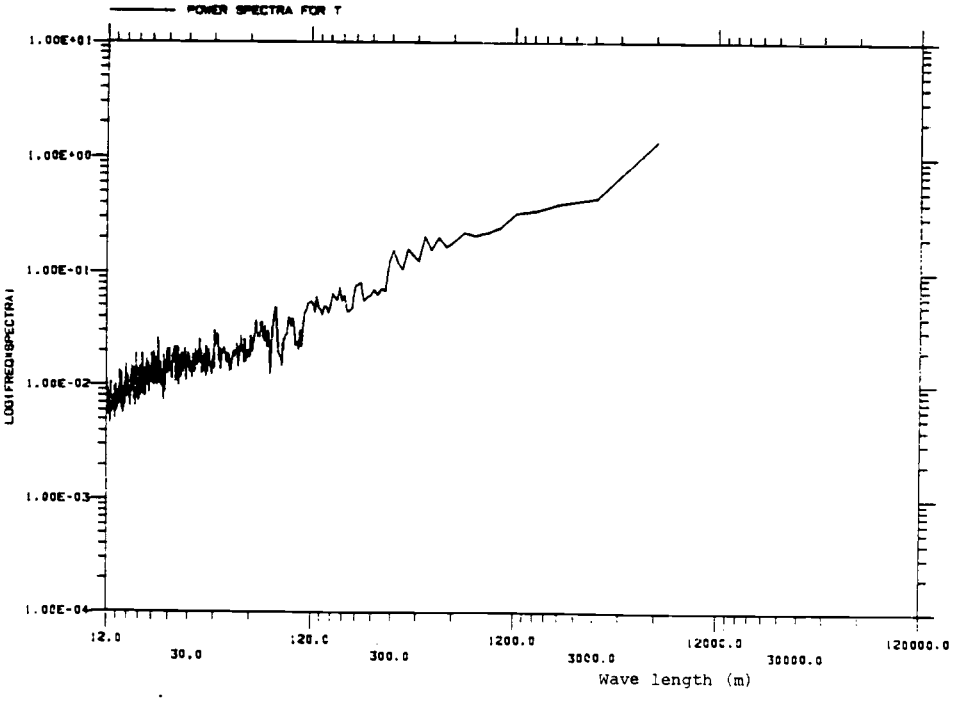

Fig. (3.1.10) Power Spectra of T

ALPEX STRONG COMPOSITE

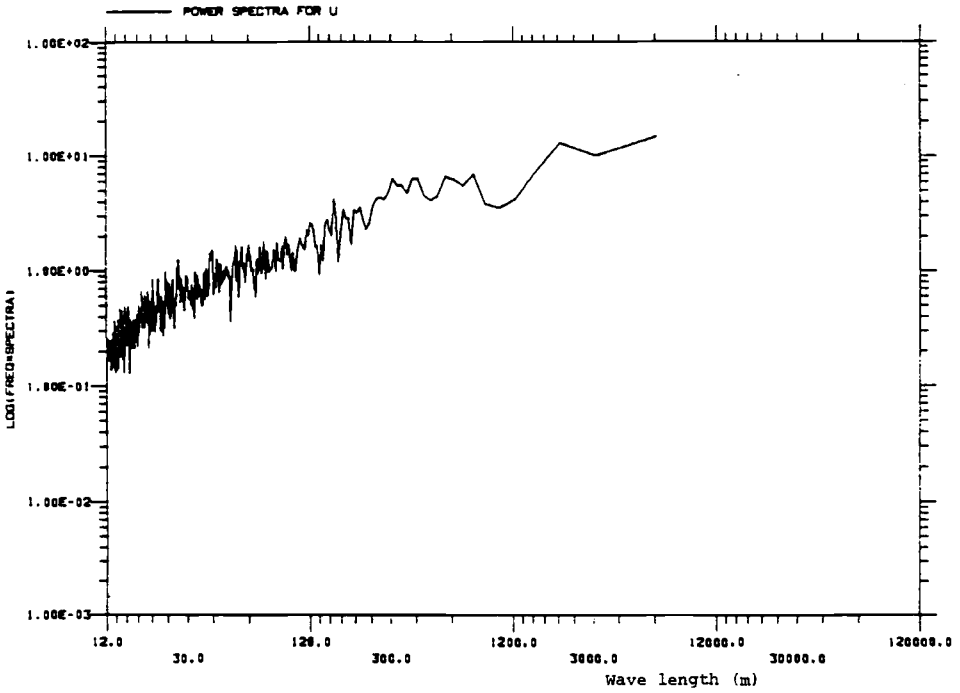

Fig. (3.1.11) Power Spectra of U

ALPEX STRONG COMPOSITE

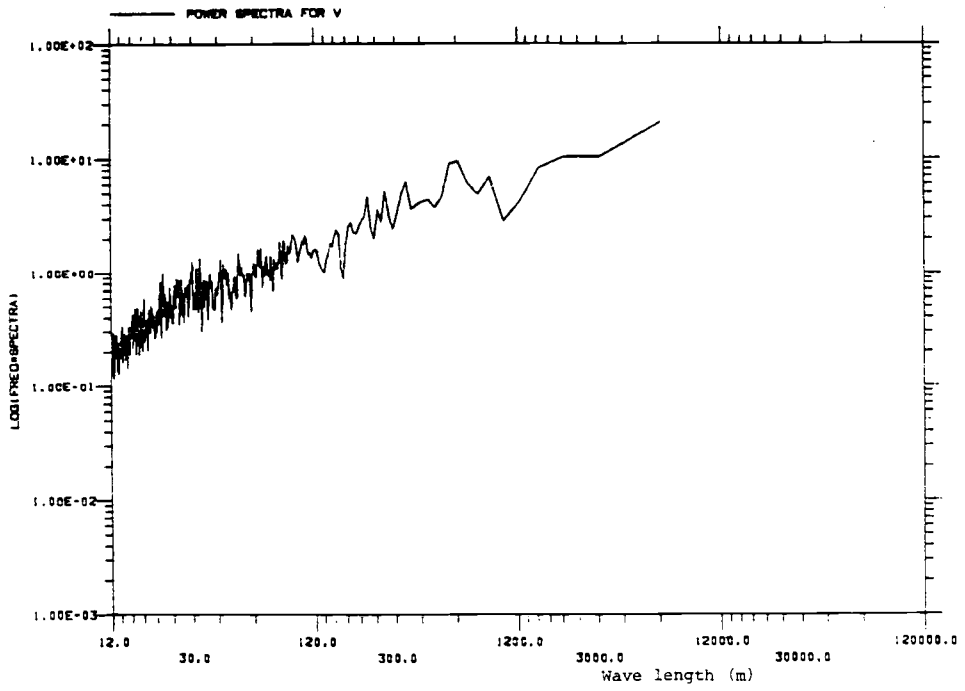

Fig. (3.1.12) Power Spectra of V

ALPEX STRONG COMPOSITE

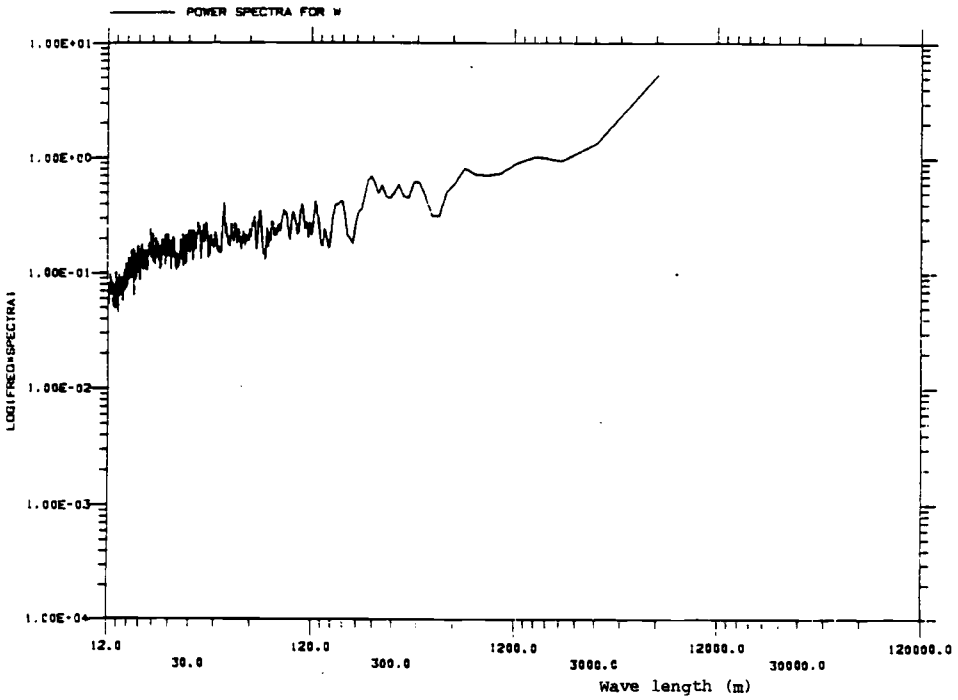

Fig. (3.1.13) Power Spectra of W

ALPEX MODERATE COMPOSITE

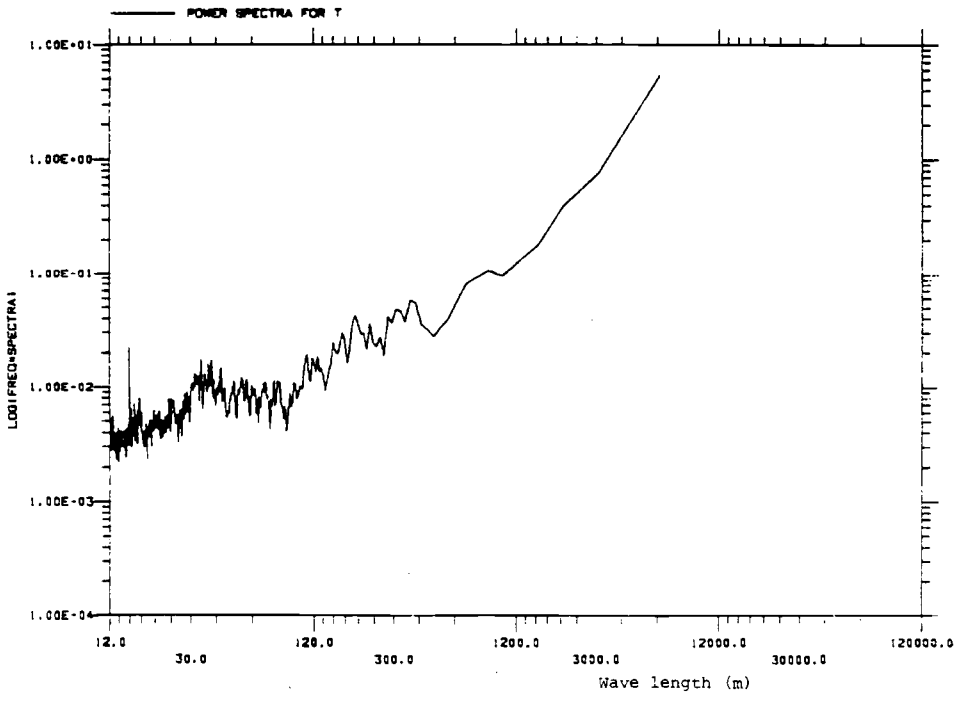

Fig. (3.1.14) Power Spectra of T

ALPEX MODERATE COMPOSITE

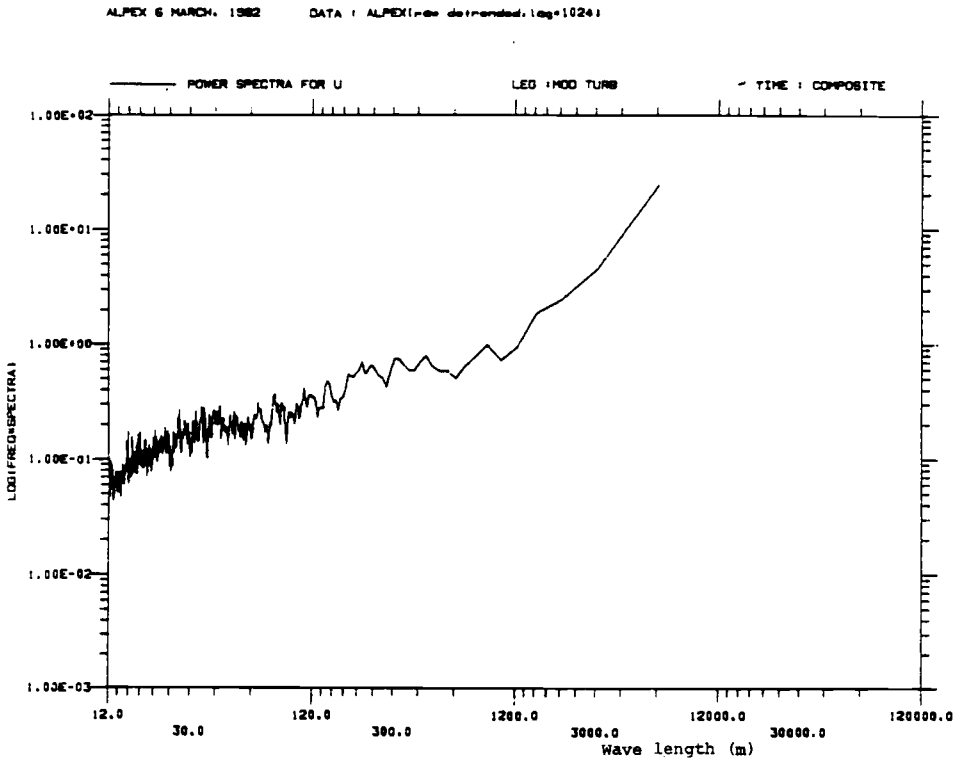

Fig. (3.1.15) Power Spectra of U

ALPEX MODERATE COMPOSITE

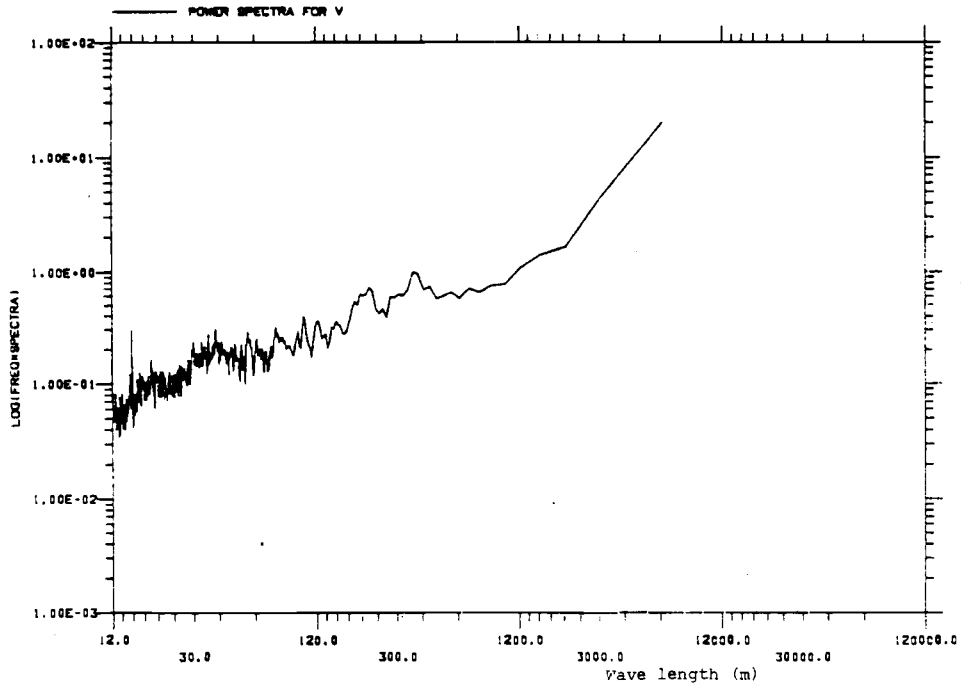

Fig. (3.1.16) Power Spectra of V

ALPEX MODERATE COMPOSITE

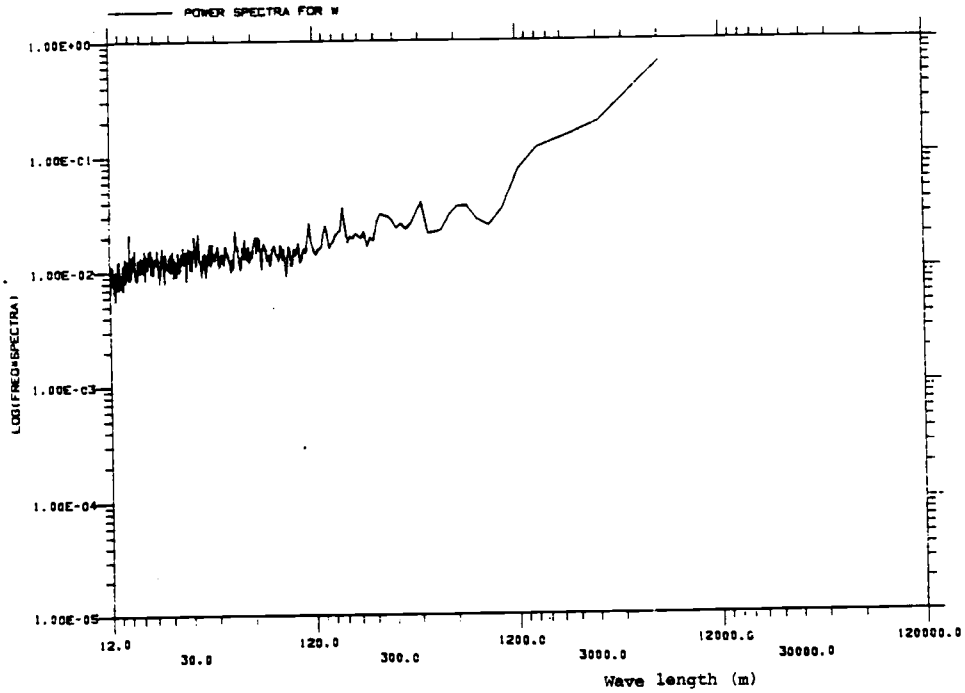

Fig. (3.1.17) Power Spectra of W

ALPEX WEAK COMPOSITE

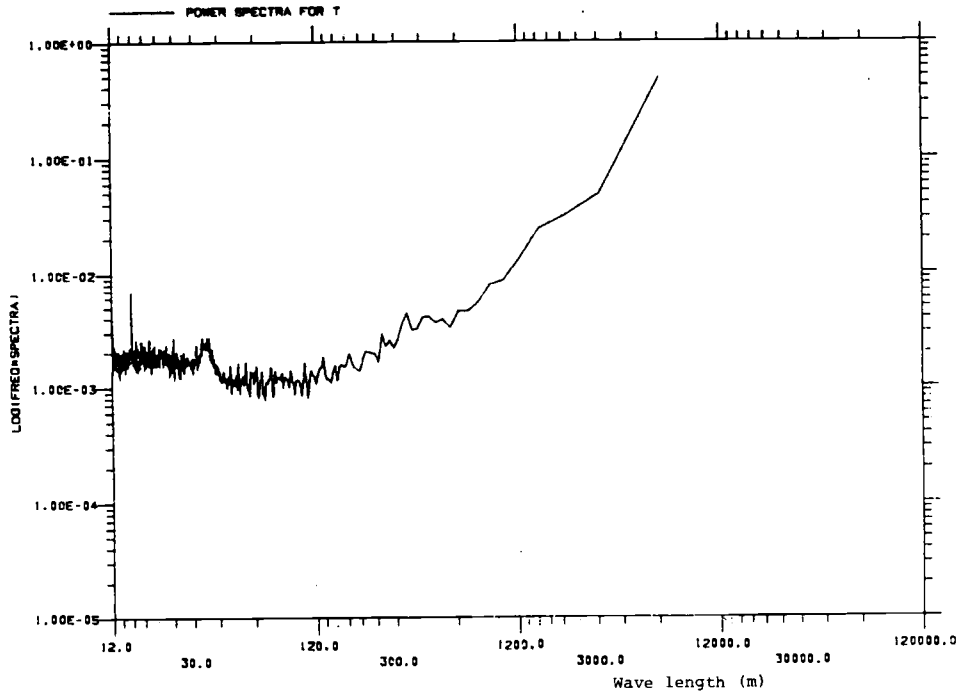

Fig. (3.1.18) Power Spectra of T

ALPEX WEAK COMPOSITE

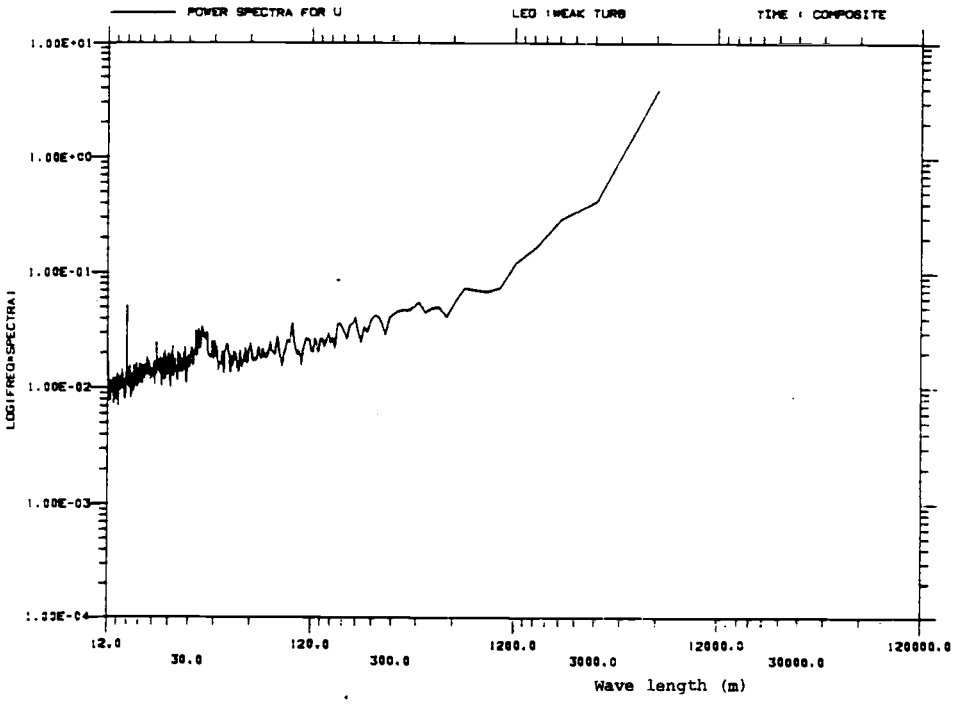

Fig. (3.1.19) Power Spectra of U

ALPEX WEAK COMPOSITE

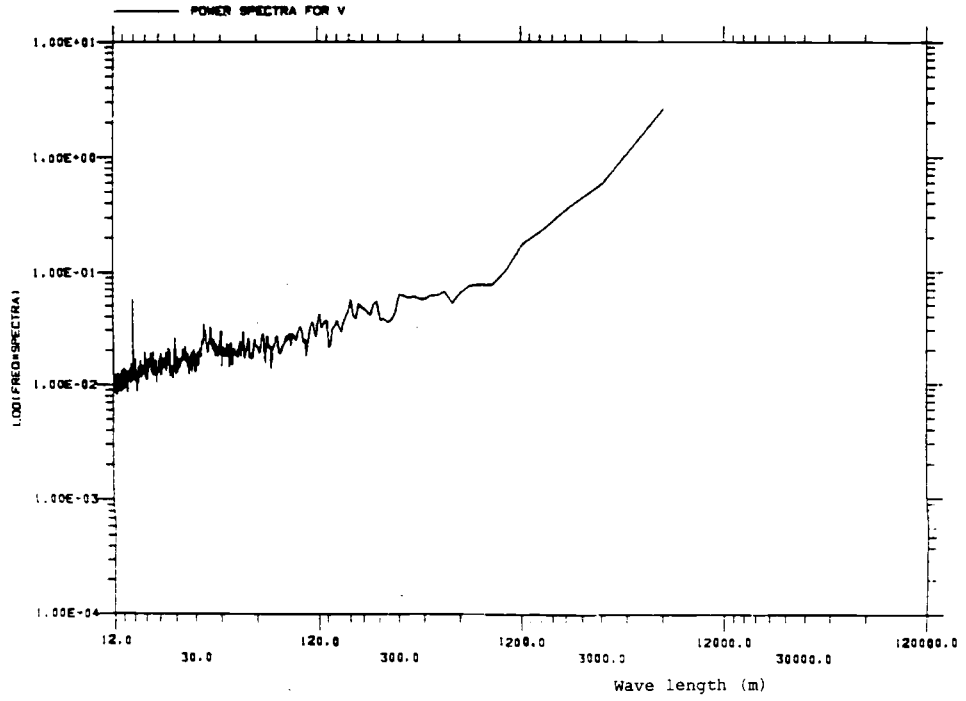

Fig. (3.1.20) Power Spectra of V

ALPEX WEAK COMPOSITE

3.2 Computation Of Statistics Of Increments.

The statistics of increments were computed on raw data as the detrending used in spectral estimation was considered redundant in view of the discussion in chapter 2. (See chapter 2 for effects of trend on computed statistics). The compositing was done at each separation distance, similar to that done at each wave length in the case of spectra.

The composite plots of the structure function are in Fig. (3.2.1 to 3.2.5). The plots have been made on a log-log scale to compare their slopes with the theoretical prediction and to facilitate easy comparison with spectra.

The co-structure function has been computed for the variable pairs WU, WV, WT, VT, UT, and UV. These are shown in fig.(3.2.6 to 3.2.15). The co-structure is plotted on a non-log scale as it may take negative values.

3.3 Computation Of Other Statistics.

In addition to the above the structure aspect ratio defined as

$$\text{Aspect ratio} = \text{sqrt.}[D_{ww}(r)/(D_{uu}(r) + D_{vv}(r))]$$

is shown in fig (3.3.1).

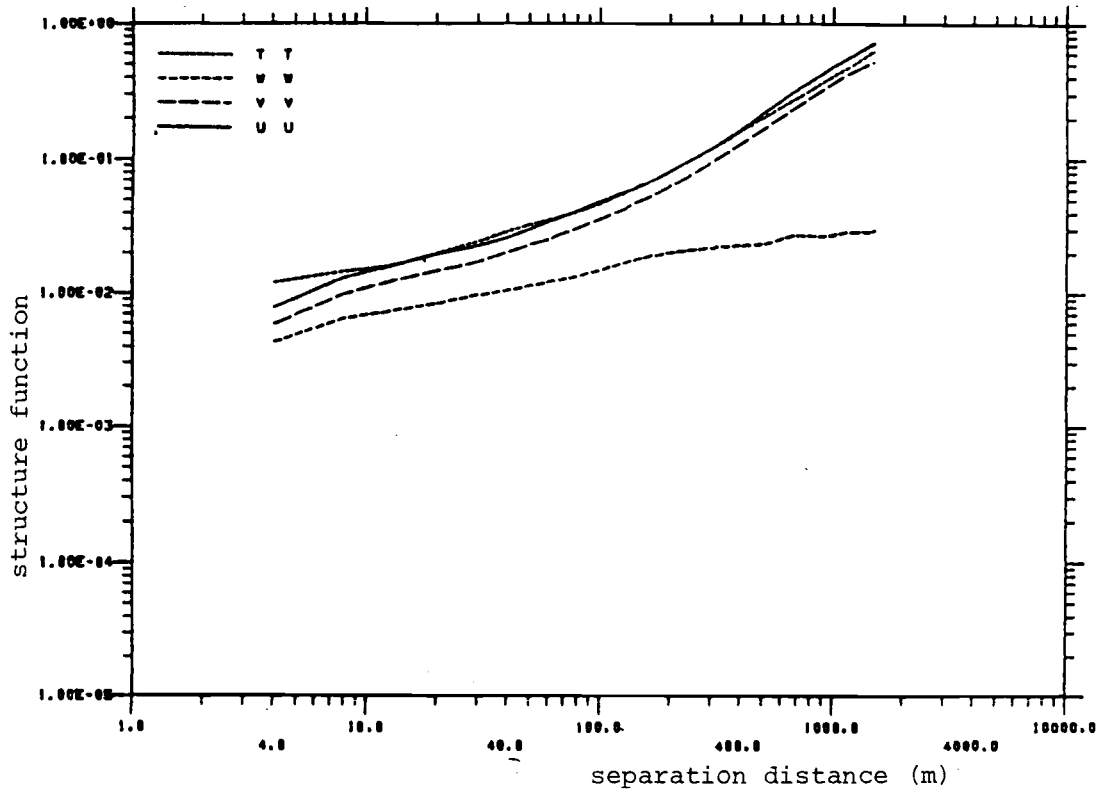

Fig. (3.2.1) Structure Functions of U, V, W and T

SESAME 5 th May

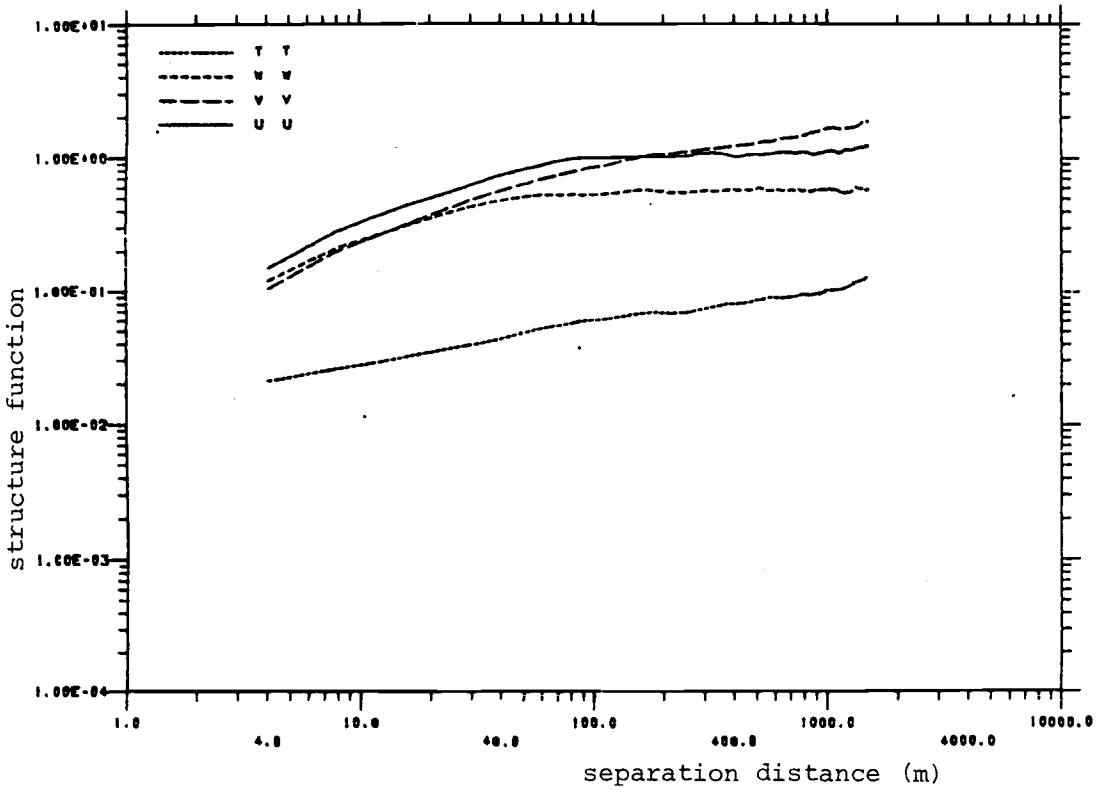

Fig. (3.2.2) Structure Functions of U, V, W and T

SESAME 6 th May

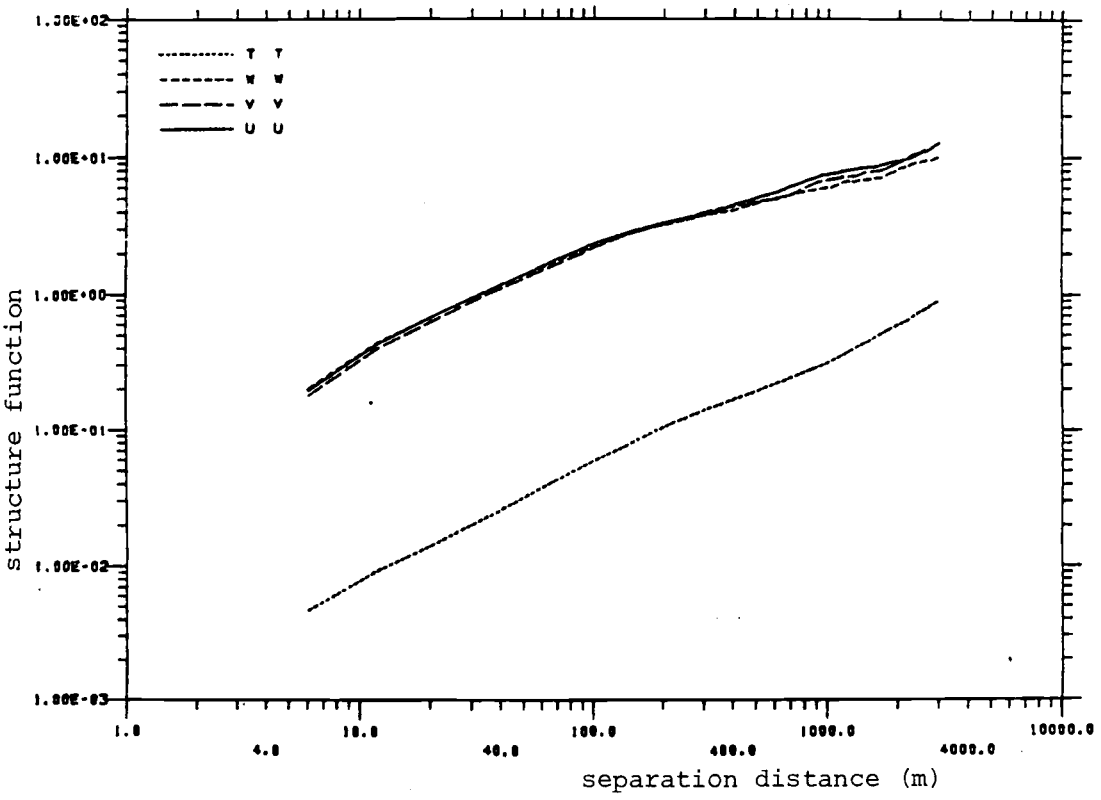

Fig. (3.2.3) Structure Functions of U, V, W and T

ALPEX STRONG COMPOSITE

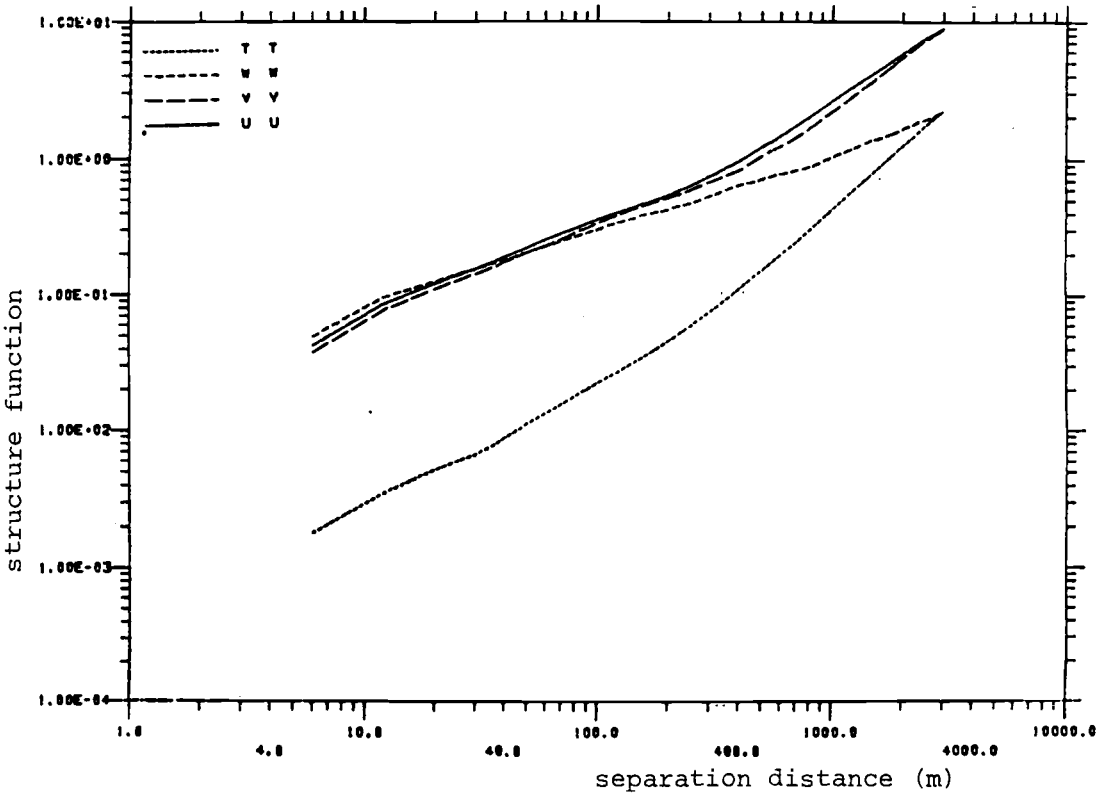

Fig. (3.2.4) Structure Functions of U, V, W and T

ALPEX MODERATE COMPOSITE

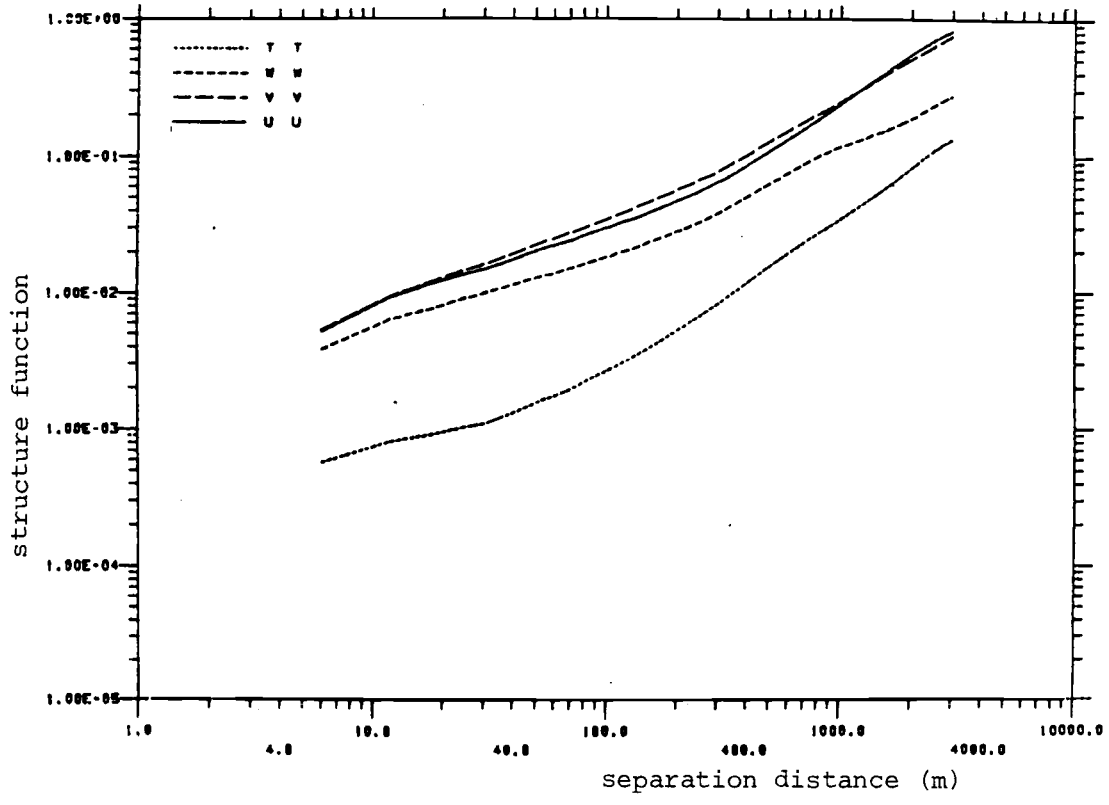

Fig. (3.2.5) Structure Functions of U, V, W and T

ALPEX WEAK COMPOSITE

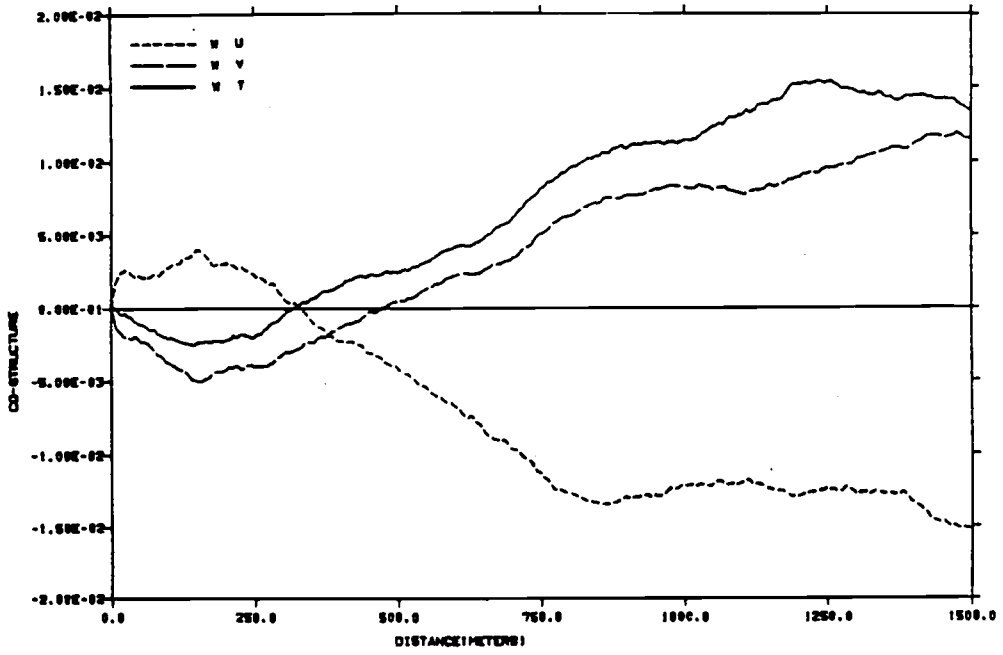

Fig. (3.2.6) Co-structure Functions of WU, WV And WT
SESAME 5 th May

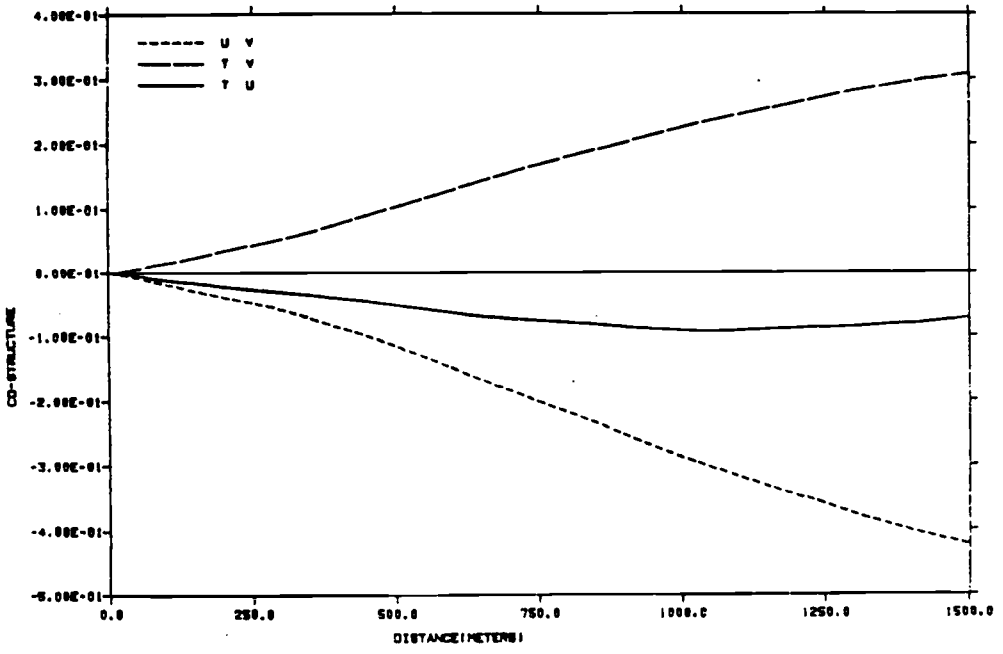

Fig. (3.2.7) Co-structure Functions of UV, UT And VT
SESAME 5 th May

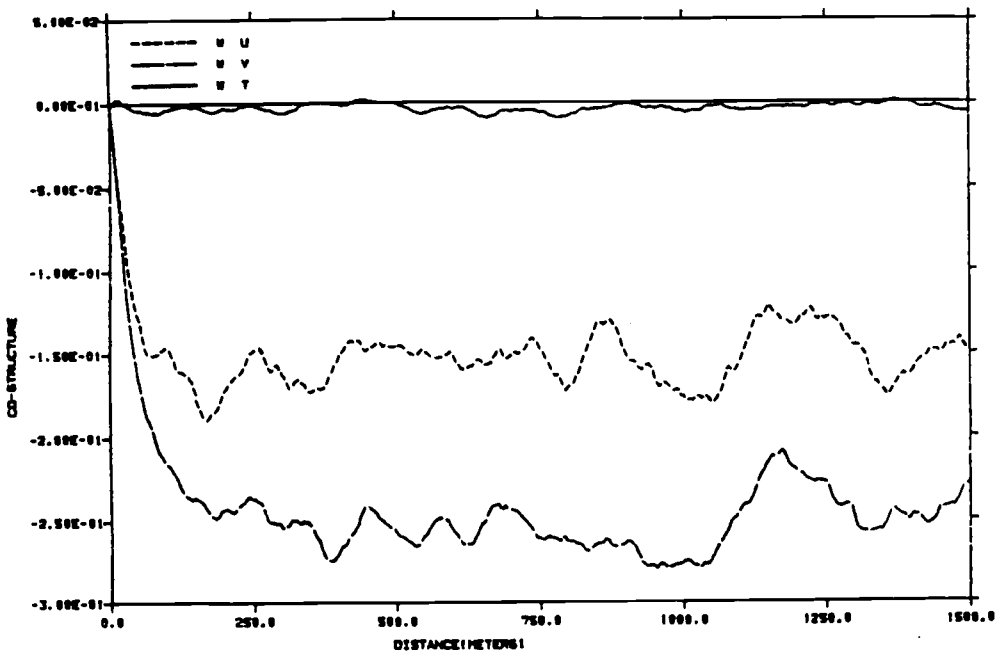

Fig. (3.2.8) Co-structure Functions of WU, WV And WT

SESAME 6 th May

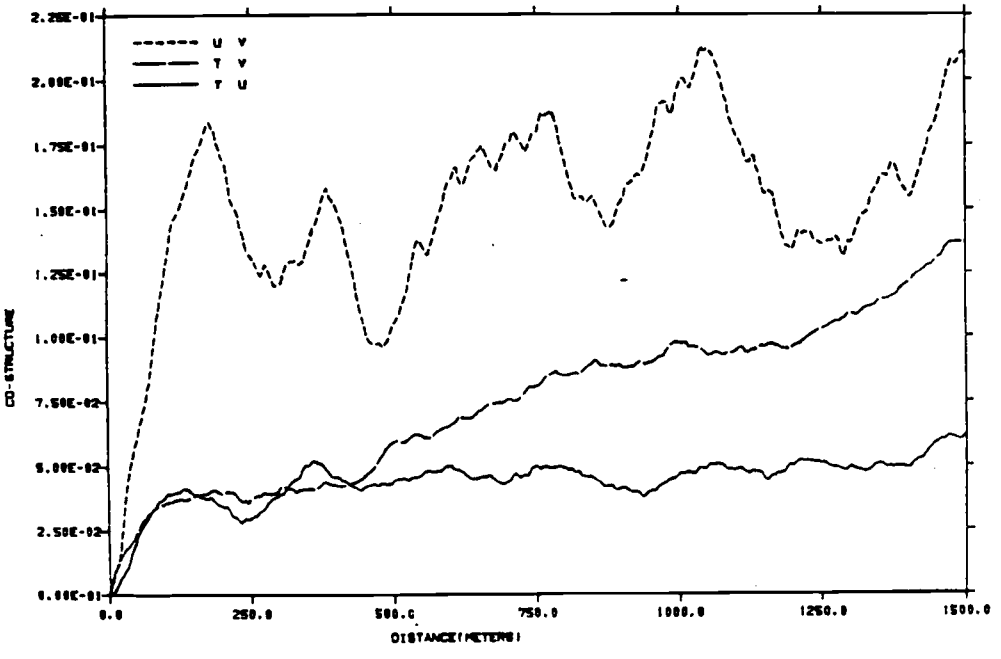

Fig. (3.2.9) Co-structure Functions of UV, UT And VT

SESAME 6 th May

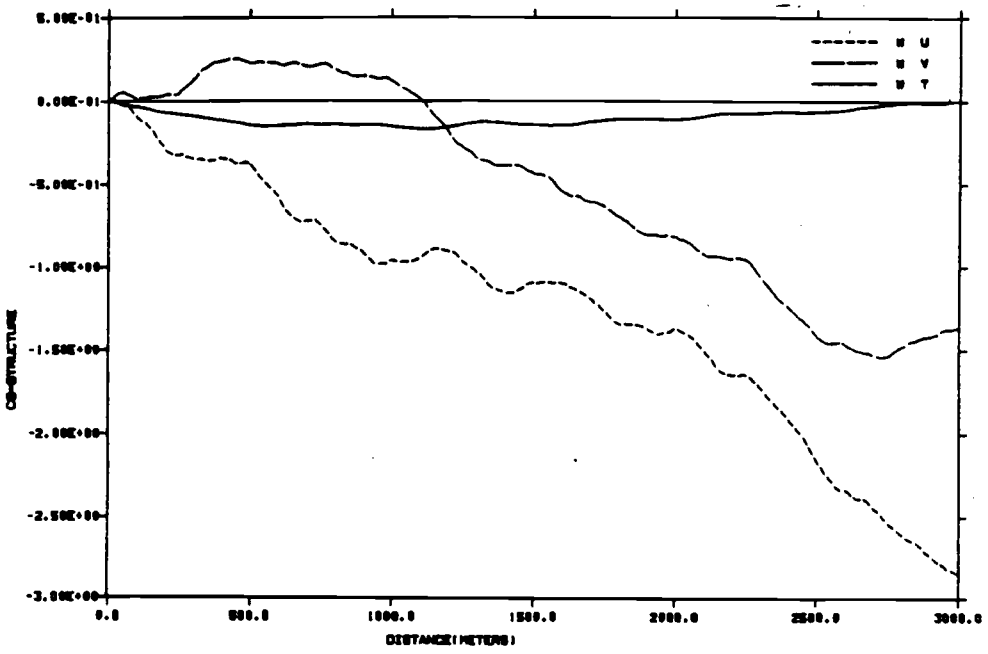

Fig. (3.2.10) Co-structure Functions of WU, WV And WT

ALPEX STRONG COMPOSITE

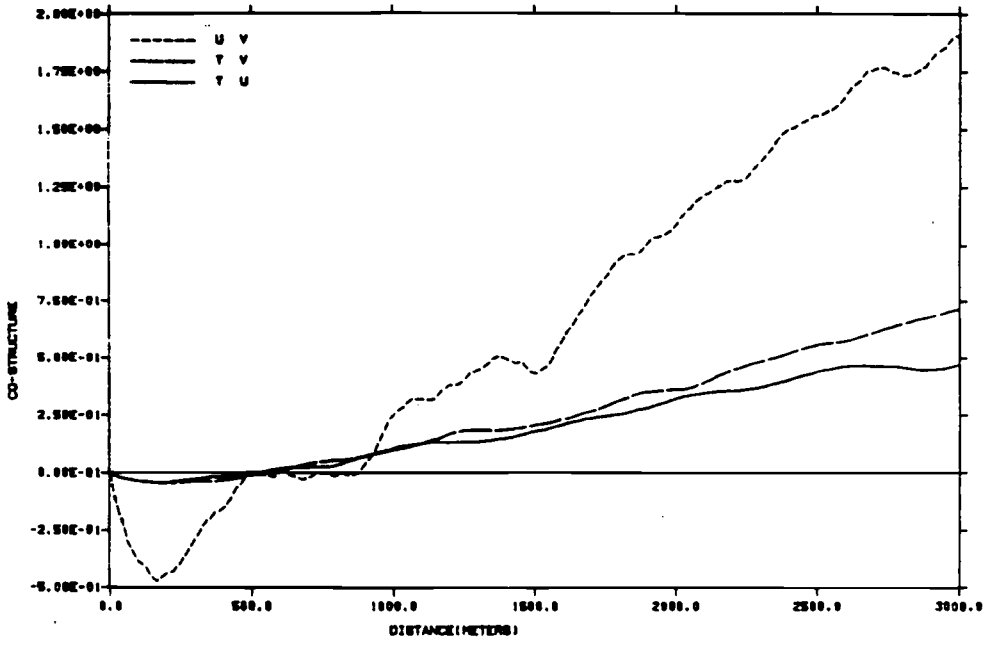

Fig. (3.2.11) Co-structure Functions of UV, UT And VT

ALPEX STRONG COMPOSITE

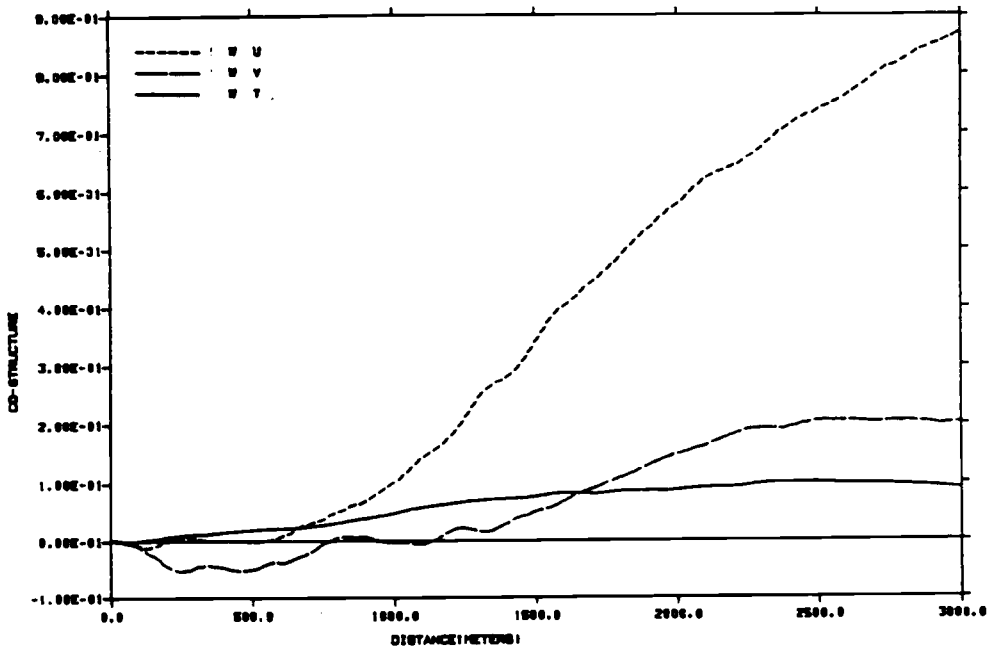

Fig. (3.2.12) Co-structure Functions of WU, WV And WT

ALPEX MODERATE COMPOSITE

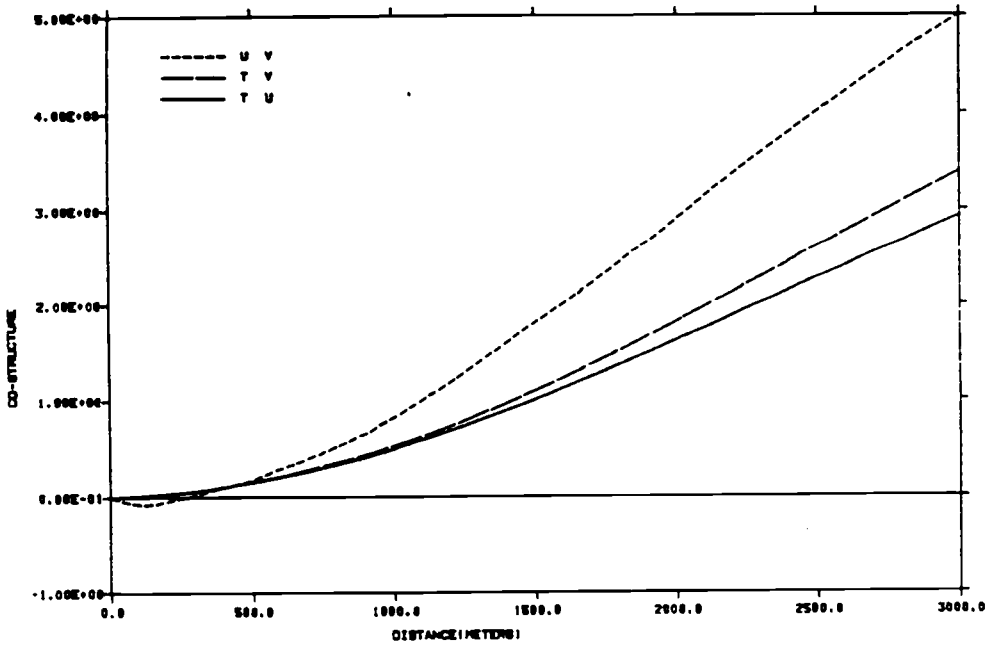

Fig. (3.2.13) Co-structure Functions of UV, UT And VT

ALPEX MODERATE COMPOSITE

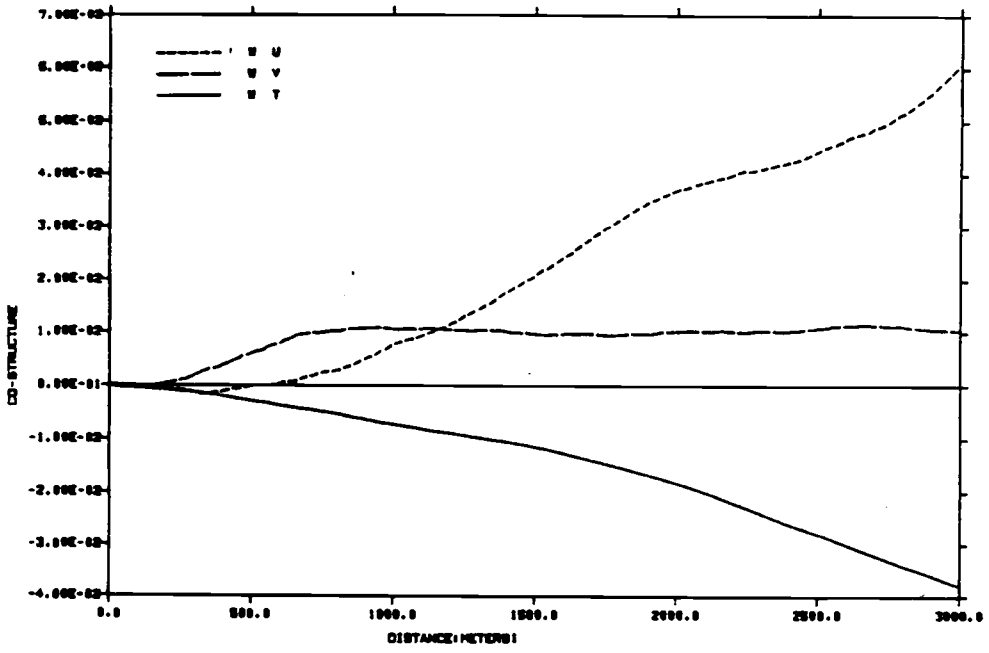

Fig. (3.2.14) Co-structure Functions of WU, WV And WT

ALPEX WEAK COMPOSITE

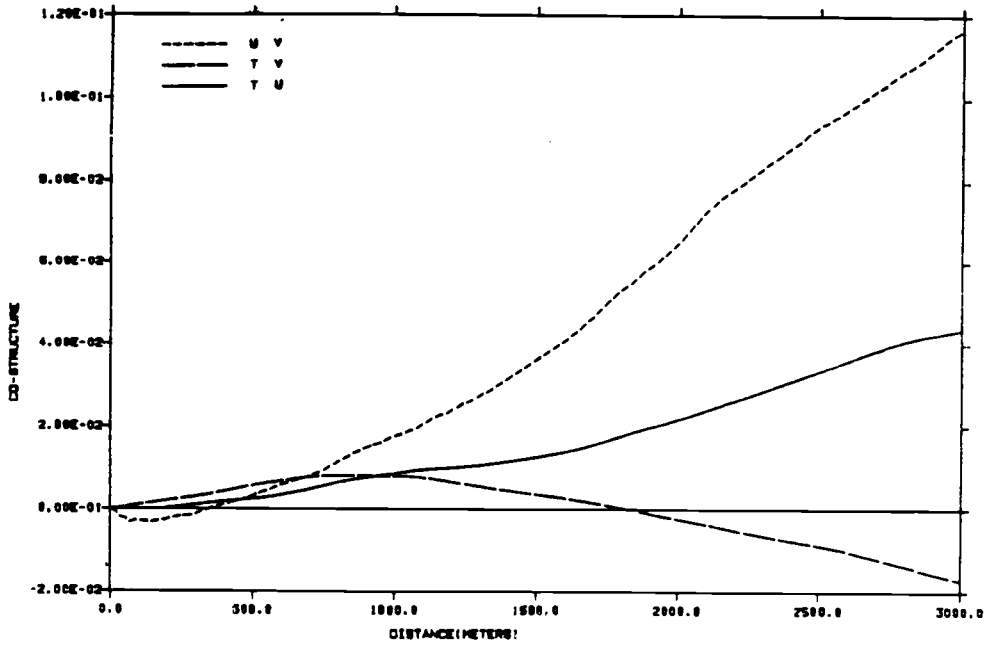

Fig. (3.2.15) Co-structure Functions of UV, UT And VT

ALPEX WEAK COMPOSITE

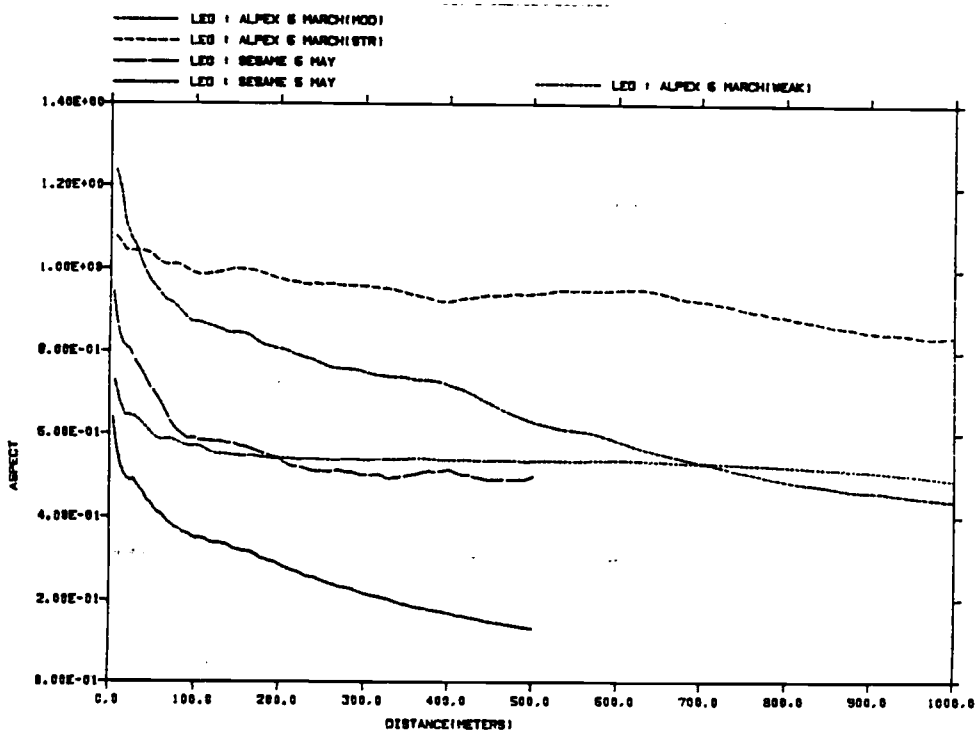

Fig.(3.3.1) Aspect ratios

4.0 DISCUSSION

Theoretically, an idealized wave of wave number k would result in a peak at k in the power spectra, and in a peak at k/2 in the structure function. Therefore one would expect to observe a shift to lower scales in the dominant features of a given data record when viewed from the structure function curves. However, a shift by a factor of two holds only for data that consist of individual sinusoids. In studies of artificially made records of square pulse type wave forms, it was seen that the spectra tend to peak at the wave number corresponding to that of the square pulse, and also had smaller peaks at higher wave numbers, while the structure function still contained a single peak at half the wave length. In general, the sharper the edges, the more spread out the spectral plots became. The structure function was less influenced by the sharp boundries.

The observed structure function plots and the power spectra plots indicate the presence of a region of -2/3 slope. While this region is barely seen in the Alpex weak composite spectra, it extends to around 3000 meters in the Alpex strong composite spectra. This region appears to scales of about 100 m in the structure function for Alpex weak composite and around 500 meters in the Alpex strong composite. This indicates that the expected shift in scales exists in the data being analysed. The shift to

lower scales is closer to a factor of 2 (the predicted value for records made up of smooth functions) in the weak turbulence case, (whereas it is around a factor of 6 for the strong turbulence) it appears that the record has lesser sharp edges than the strong turbulence.

The existence of the -2/3 region in both the structure function and the power spectra depends very much on the type of turbulence. While the -2/3 region exists for a wave band up to 3000 m in the Alpex strong turbulence case, it is virtually nonexistent in the Sesame 5th May composite, where the turbulence is extremely weak. This indicates that the growth of the inertial subrange depends on the strength of the turbulence as well as the effect of the stratification. As the shear becomes stronger and the stratification weaker, the energy cascade originates from larger energy containing eddies. This effect is seen in plots of horizontal as well as vertical velocities.

The constant ratio of lateral and longitudinal structure functions (and spectra) as predicted theoretically (For example by Townsend, 1976) is seen to be around 4/3 and agrees well with the expected value. This effect is clearly seen in the structure function plots where the structure functions of u and v run parallel through most of the inertial subrange. Due to the noise in the spectral plots, the computation of the ratio from it is ambiguous.

The plots of structure function and spectra normally indicate a steepening in slope beyond the -2/3 region. This effect is clearly seen in the Sesame 5th May and Alpex weak turbulence cases. This -2 region reduces in extent as the turbulence strengthens and apparently moves to larger scales in the strong Alpex case. (see Gage, 1985 for spectra showing a -2 region). This effect is seen in the spectra as well as in the structure function plots even though the structure functions have been computed to a lesser separation distance than the spectra. The -2 region in these plots may be due to a catch-up region where the spectra of the meso-scale activity and the turbulence is bridged. (When the energy containing eddies extend to large wave lengths as in the Alpex strong composite this catch-up region may be eleminated.)

In Sesame 6th May composite this steepening effect is not observed. This region is replaced by a region of reversed slope as would be expected by spectra of a buoyancy subrange. This may be due to the fact that the flights of 6th May were made later in the morning (after sun rise) when convective heating of the boundary layer might be of importance or due to weak meso scale activity.

The computations of aspect ratio indicate that the turbulence remains 3-dimensional to larger wave lengths, as the turbulence becomes stronger. This may be due to the shear dominating the motion and obscuring the effect of stratification. The increase in aspect ratio beyond 1 in the Alpex moderate case (at very small scales) cannot be explained and may be due to the inclusion of a bad segment in the composite.

Comparison of co-structure and co-spectra are difficult due to the extremely noisy co-spectra. However, in analysis of smoothed co-spectra the co-structure and co-spectra seem to agree.Notably, the co-structure did not indicate the expected shift to lower scales as evidenced in the structure function plots. This may be due to effect of trend (in the computation of spectra the records were linearly detrended only) or the effect of non-periodic structures in the flow. Non-periodic structures would contain no fixed phase and may not be represented by co-spectra and quadrature to a satisfactory extent.

5.0 CONCLUSION

The structure function is seen to be a versatile tool in the analysis of turbulence. It is smoother than the corresponding spectrum, and seem to contain the same information. It is seen to be affected by trend and large scale wave activity to a lesser extent than spectra. Computations of co-structure functions and co-spectra indicate that the co-structure is a better analysis technique as the co-spectra was found to be very noisy.

This data shows the existence of the Kolmogorov inertial subrange. However, the stratification and the shear is seen to have a strong influence on the extent to which it spreads in the wave number spectrum. The data also agrees well with the expected constant ratio of horizontal spectra. Computation of aspect ratios indicate that the flow becomes highly anisotropic at large wave lengths in the presence of strong stratification.

6.0 REFERENCES

Babiano, A., C. Basedevant ,and R. Sodourney, 1985: Structure functions and dispersion laws in two-dimensional turbulence. J. Atmos. Sci., 42 pp 941-949.

Barnes, S. L., and D. K. Lilly, 1975: Covariance Analysis of severe storm environments. In Preprints, 9th AMS conference on severe local storms,21-23 October 1975, Norman OK. pp 301-306.

Berkowicz, R., and L. Prahm, 1984: Spectral Representation of The Vertical Structure of Turbulence in the Convective Boundary Layer, Q. J. R. Met. Soc., 110, pp 35-52.

Dickey, T. D., and G. L. Mellor, 1979: The Kolmogoroff r 2/3 law, Phys. Fluids,22, No 6,pp 1029-1032

Doviak, R. J., and Zrnic, D. S., 1984: Doppler radar and weather observations, Academic press,458 pp.

Gage, K. S., and G. D. Nastrom, 1985: Evidence for coexisting spectra of stratified turbulence and internal waves in mesoscale atmospheric velocity fields,Seventh Symposium on Turbulence and Diffusion, Boulder, Colorado, pp 176-179

Kolmogorov, A. N., 1941: The Local Structure of Turbulence in Incompressible Viscous Fluid For Very Large Reynolds Numbers, C. R. Acads. Sci. USSR, 30, pp 301-305.

Kraichnan, R. H., 1967: Inertial Ranges in Two dimensional Turbulence, The Phy. Fluids, 10,No 7, pp 1417-1423.

Lilly, D. K., 1983: Stratified Turbulence and The Mesoscale Variability of The Atmosphere, J. Atmos. Sci., 40, 749-761.

Lumley, J. L., and H. A. Panofsky, 1964: The Structre of Atmospheric Turbulence, New York, Interscience, 239 pp.

Mahrt, L., 1985: Vertical Structure and Turbulence in the Very Stable Boundary Layer, J. Atmos. Sci, 42.

Moin, P., and John Kim, 1985: The structure of the vorticity field in turbulent channel flow. Part 1. Analyses of instantaneous fields and statistical correlations. J. Fluid Mech., 155, pp 441-464.

Monin, A. S., and A. M. Yaglom, 1975: Statistical Fluid Mechanics, Vol. 2, The MIT Press, 873 pp.

Nai-Ping, l., W. D. Neff, and J. C. Kaimal, 1983: Wave and Turbulence Structure in a Disturbed Nocturnal Inversion, Boundary Layer Met., 26, pp 141-155

Orzag, S. A., 1977: Statistical Theory of Turbulence, Fluid Dynamics, Ed. R.Balian and J.L.Paube, Gordin and Breach, London.

Panofsky, H. A., and J. A. Dutton, 1984: Atmospheric Turbulence. John Wiley and Sons, New York, 397 pp.

Tennekes, H., and J. L. Lumley, 1972: A First course in Turbulence, MIT press,300 pp.

Townsend, A. A., 1976: The Structure of Turbulent Shear Flow, Cambridge University Press.

-----, 1970: Entrainment and Structure of Turbulent Shear Flow. J. Fluid Mech., 41,pp 13-46

Turner, J. S., 1973: Bouyancy Effects in Fluids, Cambridge University Press, Cambridge, U.K., 367 pp.

Vinnichenko, N. K., 1970: The Kinetic Energy Spectram in the Free Atmosphere 1 Second to 5 Years, Tellus, 22, 158-166.

Weinstock, J., 1980: A Theory of Gaps in the Turbulence Spectra of Stably Stratified Shear Flows, J. Atmos. Sci., 37, pp 1542-1549.

------, 1978:On the Theory of Turbulence in the Boyancy Subrange of Stably Stratified Flows J. Atmos. Sci., 35, pp 634-649.

Wyngaard, J. C., W. T. Pennell, D. H. Lenschow and M. A. LeMone, 1978: The Temperature-humidity covariance Budget in the Convective Boundary Layer, J. Atmos. Sci., 35, pp 47-58

-----, and O. R. Cote, 1972: Cospectral Similarity in the atmospheric Surface Layer, Quart. J. Roy. Met. Soc. 98, 590-603.